approval by the ethical committees at the institutions, written informed consent was obtained from each patient and/or their family. Peripheral blood samples were collected from the patients and genotyping was performed as described.[8] After genetic diagnosis of PMD was made, another written informed consent for the iPS cell study was obtained from each patient and/or their family. Skin fibroblasts were collected from three patients and a healthy male control.

Genotyping of the patients

Genomic DNAs were extracted from peripheral blood samples from patients and others by using standard methods. Initial screening for *PLP1* duplication was performed by multiplex ligation-dependent probe amplification analysis by using the PLP1 Kit (P022; MRC-Holland, Amsterdam, The Netherlands) according to the manufacturer's instruction.[9] In case of *PLP1* duplication, the aberration region was confirmed by microarray-based comparative genomic hybridization (aCGH) using the Agilent Human 105A CGH Kit (Agilent Technologies, Santa Clara, CA, USA) as described previously.[8] To detect the small duplication in Patient 1, a custom array was designed using e-array, a web-based software (https://earray.chem.agilent.com/earray/), and 29 918 probes in chrX:98 000 000–104 500 000, around *PLP1*, were selected. The average interval of the probes was 217 bp in this region.

PLP1 duplication was confirmed by two-color fluorescence *in-situ* hybridization as described previously.[8] Two bacterial artificial chromosome clones, RP11–75D20 (located at Xp22.13) and RP11–832L2 (located at Xq22.2), were selected from the UCSC Human Genome Browser (http://genome.ucsc.edu/) and used as probes. The fixed metaphase and interphase spreads of the specimens were derived from patients' peripheral blood samples and generated iPS cells. The direction of the duplicated segment identified in Patient 2 was analyzed by fiber-fluorescence *in-situ* hybridization analysis as described previously.[8]

PCR and direct sequencing of all seven exons of *PLP1* was performed by standard methods using the primers reported by Hobson *et al.*[4] The designs of the primers for all exons and the breakpoint searches of the duplicated segments in Patient 1 are listed in Supplementary Table 1.

Cell culture

Human fibroblasts, the Plat-E Retroviral Packaging Cell Line (Cell Biolabs, San Diego, CA, USA), 293FT cells (Life Technologies, Foster City, CA, USA) and mouse fibroblast STO cell line (SNL) feeder cells (ECACC, Salisbury, UK) were grown in Dulbecco's modified Eagle's medium (DMEM 14247-15; Nacalai Tesque, Japan) containing 10% fetal bovine serum and 0.5% penicillin and streptomycin (Life Technologies). Human iPS cells were maintained on SNL feeder cells treated with mitomycin C in Primate ES Cell Culture Medium supplemented with 4 ng ml^{-1} recombinant basic fibroblast growth factor (# RCHEMD001; Repro CELL, Yokohama, Japan) and passaged as described previously.[7,10]

Generation of iPS cells

Disease-specific iPS cells were generated from patients' skin fibroblasts as previously described.[7] Briefly, recombinant lentivirus produced from 293FT cells, in which pLenti6/UbC/mSlc7a1 (AddGene, Cambridge, MA, USA) was transfected by use of Virapower Lentiviral Expression System (Life Technologies), was infected into cultured fibroblasts for 24 h. Then, four retroviruses produced with Plat-E Packaging Cells (Cell biolabs), in which pMXs-hOCT3/4, pMXs-hSOX2, pMXs-hKLF4 and pMXs-hc-MYC (AddGene) were transferred independently, were infected into mSlc7a1-expressing human fibroblasts. Six days after retroviral infection, the fibroblasts were placed onto mouse fibroblast SNL feeder cells (ECACC, Salisbury, UK) at the appropriate concentration. The following day, DMEM 14247-15 (Nacalai Tesque, Japan) was replaced with Primate ES Cell Culture Medium supplemented with 4 ng ml^{-1} recombinant basic fibroblast growth factor (# RCHEMD001; Repro CELL, Yokohama, Japan). Thirty days after transduction, each embryonic stem (ES) cell-like colony was individually placed onto SNL feeder cells. Each colony was tested to determine whether they had indeed acquired pluripotency. After validation,[10] three independent iPS cell clones were selected from the candidates generated from each patient's skin fibroblasts.

Validation of the pluripotency of iPS cells

Initially, alkaline phosphatase staining was performed for validation of iPS cells. Leukocyte Alkaline Phosphatase (AP) kit 86R (Sigma-Aldrich, St Louis, MO, USA) was used for this purpose.

Reactivation of endogenous pluripotency genes and the silencing of artificially induced retroviral transgenes indicated successful reprogramming of putative iPS cell clones. To confirm this, RT-PCR analysis and real-time PCR were performed as described below.

Total RNAs were extracted from iPS cells using ISOGEN (Nippon Gene, Tokyo, Japan) and contaminating genomic DNAs were removed by DNase (Takara, Ohtsu, Japan) according to the manufacturer's instructions. Subsequently, total RNAs were reverse transcribed into complementary DNAs by using the Superscript VILO cDNA Synthesis Kit (Life Technologies) according to the manufacturer's instructions.

Quantitative real-time PCR was performed for *OCT3/4*, *SOX2*, *KLF4*, *C-MYC*, *NANOG*, *REX1*, *GAPDH* and actin beta using the Power SYBR Green PCR Master Mix (Life Technologies) and analyzed with the 7300 Real-Time PCR System (Life Technologies). Primer sequences are shown in Supplementary Table 1.

Immunocytochemistry was also performed for all putative iPS cells. For this purpose, the following primary antibodies were used: anti-SSEA4 (1:200, MAB1435, R&D systems, Minneapolis, MN, USA), anti-OCT3/4 (1:200, AF1759, R&D systems), anti-TRA-1-60 (1:200, MAB4360, Millipore, Billerica, MA, USA), and Anti-TRA-1-81 (1:200, MAB4381, Millipore). Secondary antibodies included Alexa488-conjugated donkey anti-mouse IgG, Alexa488-conjugated goat anti-mouse IgM, and Alexa594-conjugated donkey anti-mouse IgG (1:1000, Life Technologies). Nuclei were stained with Hoechst 33342 (1:1000, Life Technologies).

Validation of the differentiation ability of iPS cells

Determination of the differentiation ability of established iPS cells is important for the selection of putative iPS cell clones. To confirm their pluripotency to differentiate into three embryonic germ layers, we used floating cultivation to form embryoid bodies as described previously.[10] iPS cells were grown as floating cultures for 8 days. After embryoid body formation, the cells were cultured on gelatin-coated dishes for an additional 8 days.

Immunocytochemistry was performed to confirm expression of the three germ layers as described elsewhere.[10] In this case, three primary antibodies were used; anti-βIII tubulin (1:1000, MRB435P, Covance, Princeton, NJ, USA) as the ectoderm marker, anti-α smooth muscle actin (1:200, A2547, Sigma-Aldrich) for mesoderm, and anti-αAFP (1:100, A8452, Sigma-Aldrich) for endoderm. Donkey anti-mouse IgG labeled with Alexa Fluor 594 and donkey anti-rabbit IgG labeled with Alexa Fluor 488 (1:1000, Life Technologies) were used as secondary antibodies. Nuclei were stained with Hoechst 33342 (1:1000, Life Technologies) for nuclear staining.

Validation of the karyotypes of iPS cells

To check the artificial chromosomal rearrangements, conventional G-banding by trypsin treatment stained with Giemsa and aCGH analyses using the same methods described above were performed for the generated iPS cell clones. iPS cell lines that acquired chromosomal rearrangements were eliminated from this study.

Database analysis

Preliminary gene expression analysis was performed using online data sets. Two microarray data sets, GSM242095 for adult human dermal fibroblasts and GSM241846 for iPS cells (clone 201B7),[7] were retrieved from NCBI Gene Expression Omnibus (GEO) and analyzed using GeneSpring GX10 (Agilent Technologies).

Northern blotting

The full-length mRNA of PLP1 (920 bp) and a partial sequence of actin beta (ACTNB; MIM #102630) mRNA (91 bp) were amplified by RT-PCR by using Human Brain Total RNA (#636530, Clonetech, Mountain View, CA, USA) as a template. Primer sequences are listed in Supplementary Table 1. The PCR product was subcloned into pGEM-T Vector System (Promega, Madison, WI,

USA) and grown in LB Broth overnight. Plasmid DNAs were extracted by an automated DNA isolation system, PI-80X (Kurabo, Osaka, Japan). DNA inserts were digested with *Sac*I and *Sac*II restriction enzymes. Following agarose gel electrophoresis, product bands were excised and extracted using the QIAquick Gel Extraction Kit (QIAGEN, Hilden, Germany). The DNA fragments were then labeled using [α-^{32}P] dCTP (PerkinElmer, Waltham, MA, USA) and used as probes for northern blotting.

Hybridization was performed as described previously.[11] Briefly, 30 μg of total RNA was extracted using ISOGEN (Nippon Gene, Tokyo, Japan) according to the manufacturer's instructions, separated on a 1% agarose/0.6 M formaldehyde gel, visualized using Radiant Red RNA Stain (Bio-Rad, Hercules, CA, USA), transferred to a nylon membrane and subsequently hybridized for 24 h with either *PLP1* or *ACTNB* probes. Images were captured using the FLA-5100 scanner (Fujifilm, Tokyo, Japan).

Initial analysis included seven samples: mitomycin-treated and -untreated SNL feeder cells, Epstein-Barr virus-infected immortalized lymphocytes derived from a normal human control, human skin fibroblasts derived from the normal control, iPS cells generated from the normal human control and two brain samples purchased from a provider (Human Fetal Brain Total RNA #636526 and Human Brain Total RNA #636530, Clonetech). Subsequent analysis included the 12 iPS cell lines generated in this study.

RESULTS

Clinical features

Patient 1 was a 16-year-old male, born by spontaneous delivery at 40 weeks gestation, with a weight of 3054 g. Soon after birth he showed nystagmus. At 4 months, he exhibited poor neck control and was diagnosed with spastic paraplegia. Psychomotor development was moderately delayed with walking alone at his age of 2 years and his intelligence quotient was estimated below 50. At 15 years, he was prescribed medication for depression. At that time, his fine motor ability allowed the use of chopsticks but he needed a wheel chair to move. His speech was dysarthric. One month later, he had an epileptic attack and was admitted to the hospital. An electroencephalogram revealed occipital spikes. Although auditory brain response was normal, brain magnetic resonance imaging (MRI) revealed a pattern of mild dysmyelination (Figures 1a and b).

Patient 2 was a 46-year-old male with two healthy female siblings. As he lacked neck control at 1 year of age, he was diagnosed with spastic cerebral palsy. Then, at 4 years, he could turn over but could not sit unaided. He lacked the ability to speak effectively, being limited to two-word sentences. At 15 years, he could use a wheel chair by himself. Subsequently, the quality of his daily life declined gradually. At 39 years, MRI revealed atrophic white matter displaying dysmyelination (Figure 1c). At present, he can move only his upper body very slowly and is bedridden. He is able to comprehend what his siblings say, but he is severely dysarthric and is able to speak only a few words very slowly.

Patient 3 was a 32-month-old boy with a birth weight of 3869 g delivered at 39 weeks gestation. He has a healthy brother. Owing to respiratory problems since birth, he was intubated and tracheostomy was performed at 58 days. He also required tube feeding. He is currently bedridden and has continuous nystagmus. Auditory-brain-response audiometry showed no waves after the first wave. A brain MRI revealed high-intensity lesions of the white matter in a T2-weighted image, indicating severe hypomyelination (Figure 1d).

Molecular analyses

Initial multiplex ligation-dependent probe amplification analysis using a PLP1 Kit (P022; MRC-Holland) identified duplications of *PLP1* in Patient 1 and 2 (data not shown).[9] Patient 2 had a duplication of all 7 exons of *PLP1*, and subsequent aCGH analysis

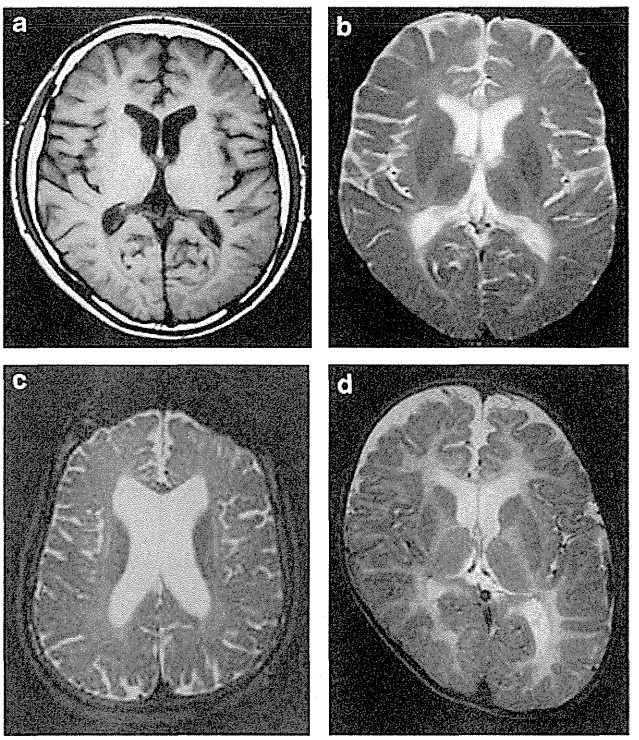

Figure 1 Brain MRI findings of the patients T1- (**a**) and T2 (**b**) weighted images of Patient 1 show mild and diffuse volume loss of the brain and high-intensity signals of the deep white matter in T2 indicating mild dysmyelination. T2-weighted image of Patient 2 (**c**) shows diffuse volume loss resulting in the dilatation of the ventricles and dysmyelination in the white matter. T2-weighted image of Patient 3 (**d**) shows extremely hypomyelinated pattern with high intensity in all white matter.

by using the Human Genome CGH Microarray 105 K (Agilent Technologies) revealed that the duplicated region was chrX:102 519 000–103 155 851 (636 851 bp) with an average $\log_2$ ratio of +0.83, which is a typical duplication region seen in PMD patients with *PLP1* duplications (Figure 2a). The duplication was confirmed by fluorescence *in-situ* hybridization (Figure 2b), and the direction of the duplicated segment, including *PLP1*, was shown to be in a tandem configuration by fiber-fluorescence *in-situ* hybridization analysis (Figure 2c).

The duplication identified in Patient 1 was unique because only the first 3 exons (exons 1–3) of *PLP1* were included in the duplicated region. To confirm this partial duplication, we designed a custom aCGH chip and used it to detect the precise duplication region. As shown in Figure 3a, the duplicated region was chrX:102 912 361–102 928 360 (15 999 bp) with an average $\log_2$ ratio of +0.72. To determine the location of the duplicated segment, we sought to detect the breakpoint by PCR direct sequencing, using primers A and B (Supplementary Table 1). A 775-bp band was obtained and re-sequenced (Figures 3b and c). Ultimately, an extremely small duplication of 16 208 bp, which has never been previously reported, was identified. The sample from Patient 1's mother was also analyzed and she was found to be a carrier of this duplication (Figures 3b and c).

In Patient 3, a novel missense mutation, c.636G>C (W212C), was identified in exon 5 of *PLP1* (Figure 2d). The *PLP1* sequence is completely conserved among species and this novel mutation was not identified in 100 normal control samples (50 males and 50 females). This patient's mother declined to have her genotype analyzed.

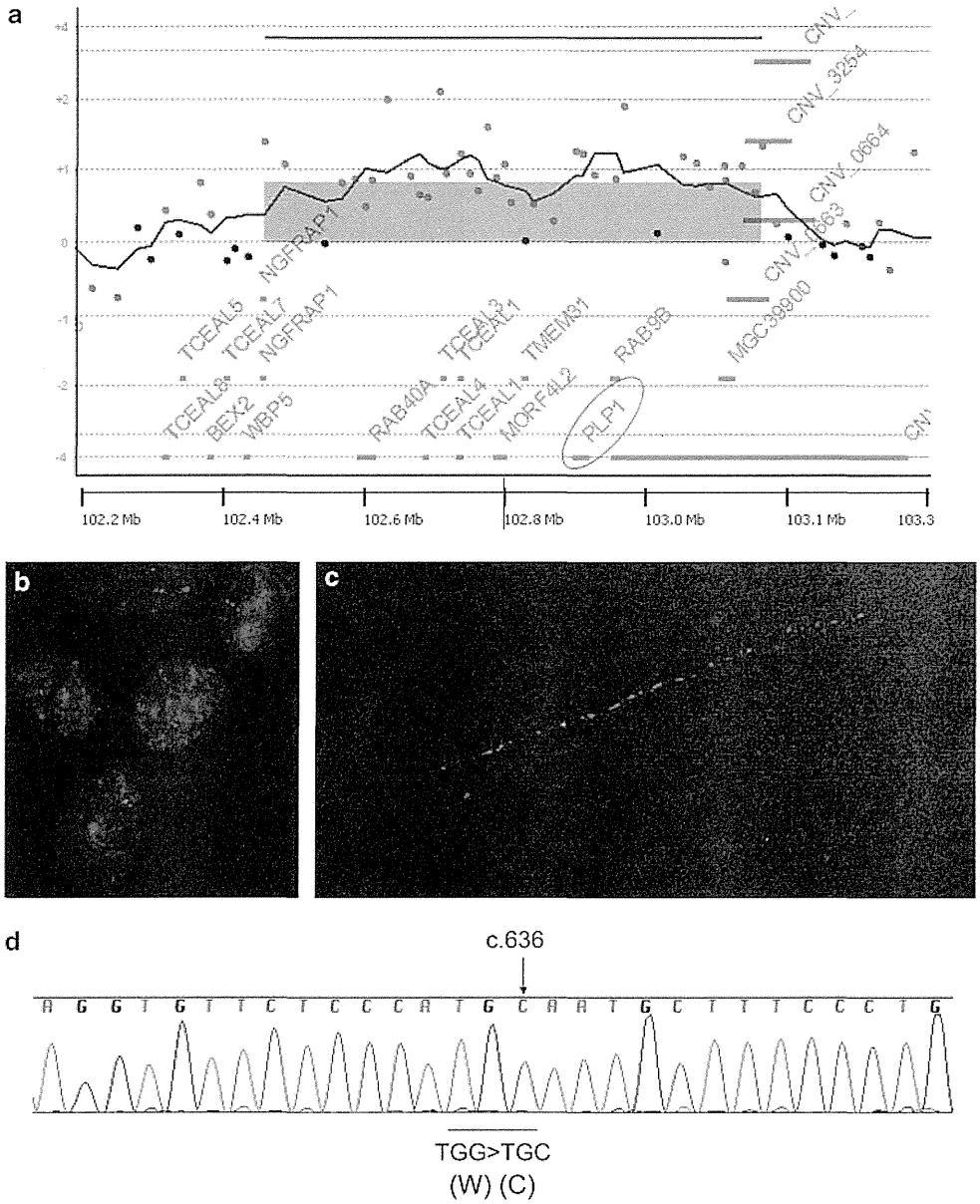

Figure 2 Genotyping and cytogenetic analyses for Patients 2 and 3. (**a**) A microchromosomal duplication including *PLP1* is shown in GeneView of Agilent Genomic Workbench (Agilent Technologies). The location of *PLP1* is highlighted by a red circle. (**b**) Interphase fluorescence *in-situ* hybridization analysis shows two green signals labeled on RP11-832L2 (located at Xq22.2) in the nucleus. Red signals labeled on RP11-75D20 (located at Xp22.13) are the marker for X chromosome. (**c**) Fiber-fluorescence *in-situ* hybridization analysis indicates tandem configuration of the duplicated segments labeled with green and red probes. (**d**) Electropherogram shows a novel missense mutation c.636G>C (W212C) in Patient 3.

Generation of iPS cells

We successfully generated iPS cells from three patients with PMD and a normal male control (Supplementary Figure 1). At least three independent clones were validated using the following three categories: (1) silencing of four transfected genes (*OCT3/4, C-MYC, KLF4* and *SOX2*; Supplementary Figure 2); (2) expression of endogenous pluripotency genes (*OCT3/4, SOX2, KLF4, C-MYC, NANOG* and *REX1*; Supplementary Figures 3 and 5); and (3) confirmation of the differentiation potency by immunocytochemistry (Supplementary Figure 4). Karyotype and aCGH analyses for the resulting iPS cells showed no artificial chromosomal rearrangements.

PLP1 expression

Preliminary *PLP1* expression levels were compared between two online data sets for human skin fibroblasts and iPS cells. The results showed that *PLP1* expression levels were $\times 40.70$ ($\log_2 = 6.38$) higher in iPS cells than in skin fibroblasts (Supplementary Figure 6). Subsequently, our initial experiments for *PLP1* expression in several samples were performed by northern blot analysis, which revealed predominant *PLP1* expression in the brain (fetal brain had weaker expression than adult brain). Although the other samples showed no *PLP1* expression, we could detect the *PLP1* band in iPS cells (Figure 4); the differentiation between two isoforms for *PLP1* and *DM20* could not be detected owing to small size differences as same as

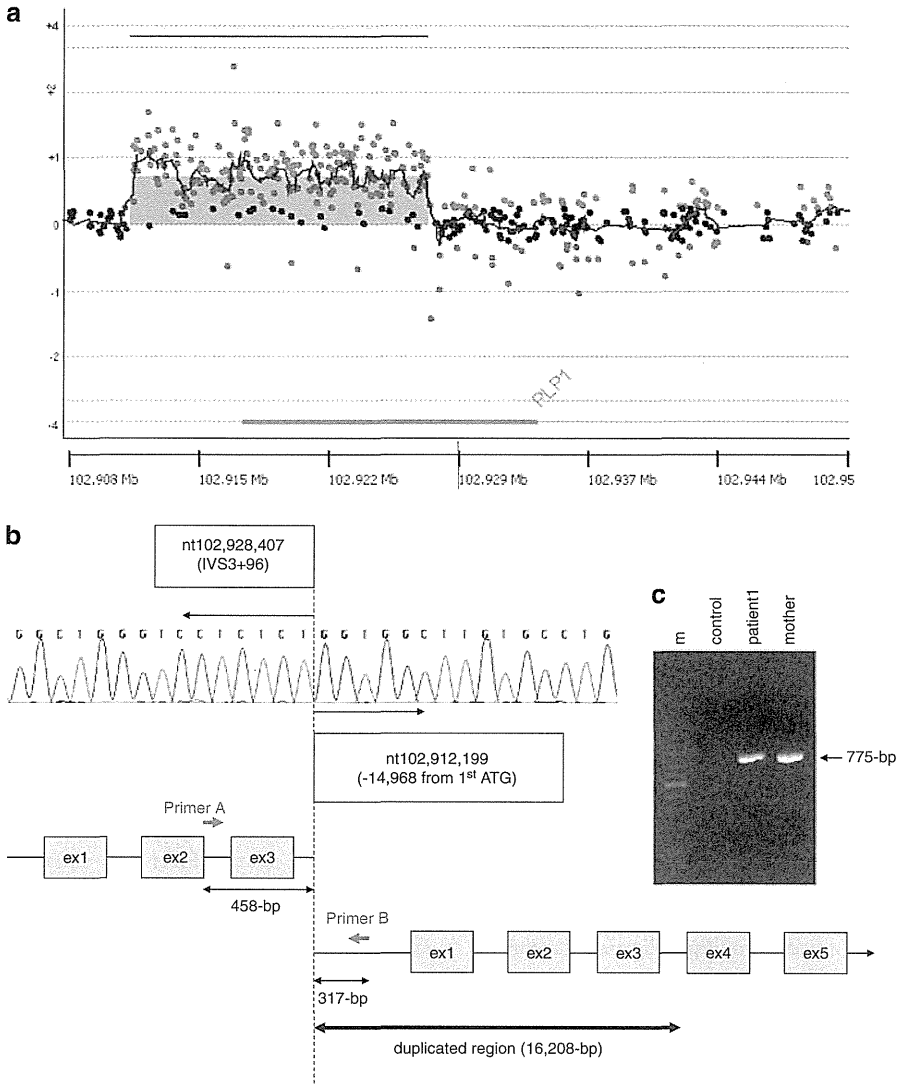

Figure 3 Molecular analyses of the *PLP1* duplication identified in Patient 1. (**a**) The result of a custom-designed aCGH shows partial duplication of *PLP1*. (**b**) A schematic representation of the breakpoint analyzed by PCR and subsequent sequencing. (**c**) A 775 bp PCR product including a breakpoint is amplified by Primer A and B and is shown in electrophoresis. m; molecular marker OneSTEP Ladder 50 (Nippon Gene).

the previous study.[12] Finally, total RNA samples extracted from the 12 iPS cell clones generated in this study were analyzed. Although we could detect the *PLP1* band in iPS cells from normal individual and Patients 2 and 3, we could not detect the *PLP1* band in the iPS cells generated from Patient 1, indicating null expression of *PLP1* caused by the partial duplication of *PLP1* (Figure 5). In Patients 2 and 3, *PLP1* signals appeared to be somewhat stronger than in controls, but because of the large variation in signal intensity among different cell lines, it was inconclusive in our limited experiments.

DISCUSSION

In this study, we identified different *PLP1* abnormalities in three patients with PMD. Patient 3 showed a novel missense mutation, c.636G>C (Tyr212Cys), which is in the extramembrane region of the PLP1 protein.[2] A missense substitution in the same codon, but resulting in a change into a different amino acid, c.634T>C (Tyr212Arg), has been reported to be a pathogenetic mutation by others.[13] Frequently, a cysteine residue changes the three-dimensional protein conformation drastically owing to disulfide bond formation with other cysteines.[14] Thus, the amino-acid substitution to cysteine in our patient is likely a pathogenetic mutation, causing PMD. Previous genotype-phenotype correlation study showed that the phenotype of patients with *PLP1* missense mutations was more severe than those with *PLP1* duplications.[1–3] Indeed, Patient 3 showed severely delayed psychomotor development complicated by respiratory and feeding difficulties. His condition can be classified as form 0 according to the classification proposed by Cailloux *et al.*,[13] as form 0 is the most severe form of PMD. Dysmyelination in this patient was particularly severe.

Patient 2 had a 0.6-Mb duplication including *PLP1*. This size is typical for PMD patients with *PLP1* duplications.[8,15,16] This patient is now 43 years old and does not show any deterioration of neurological abilities. Despite being bedridden, he can verbally communicate with several words. His clinical condition can be classified as form 2, because his maximum motor ability was sitting. His dysmyelination is milder than that of Patient 3.

The most intriguing result in this study is the partial duplication of *PLP1* identified in Patient 1. Although there have been reports

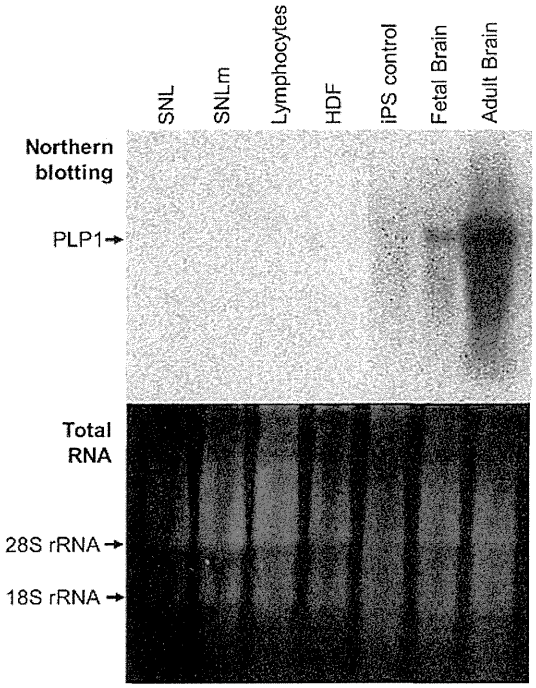

Figure 4 *PLP1* expression analysis by the northern blotting for various samples. (Upper) Predominant expression of *PLP1* is shown in the brain samples. Although control iPS cells show weak expression, there are no expressions of *PLP1* in the other samples. (Bottom) Agarose gel staining for the total RNAs before subsequent northern blotting indicates the same amounts of total RNAs loaded in each lane. SNLm, SNL-feader cells treated with mitomycin; HDF, human dermal fibroblasts

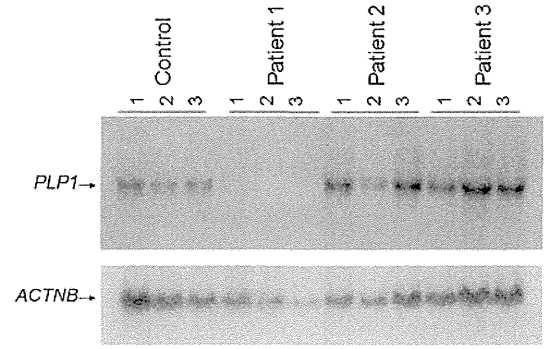

Figure 5 *PLP1* expression analyses using northern blotting. Three iPS cells of Patient 1 show no *PLP1* band, whereas the other iPS cells from normal control, Patient 2 and Patient 3 show expressions of *PLP1*. *ACTNB* (actin beta) is used for internal control.

of partial deletions in *PLP1* identified by multiplex ligation-dependent probe amplification analysis,[9] this is the first report of a partial duplication of *PLP1*. The duplicated segment included the promoter region and the first three exons. Therefore, we hypothesized that a very short mRNA or long fusion mRNA might be expressed by this duplication together with the normal mRNA. To confirm this hypothesis, we analyzed *PLP1* expression by using northern blot analysis, the only way to detect the length and the quantity of mRNAs. As expression levels of *PLP1* in skin fibroblasts were too low to be examined by northern blot analysis, we generated iPS cells from the patients. Contrary to expectation, northern blot analysis showed no *PLP1* bands in the iPS cell generated from the fibroblasts of Patient 1. Although there may be a limitation to detect short-unstable mRNAs in our method, this possibly indicated that the expression of *PLP1* mRNA was disturbed by the *PLP1* partial duplication identified in Patient 1. Regarding the clinical severities of the patients, Patient 1 showed milder phenotype than Patient 2, and his condition can be classified as form 3. Previous genotype-phenotype correlation study have shown that patients with *PLP1* missense mutations show severe manifestation associated with severe hypomyelination, which is recognized as the consequence of accumulated mutant protein in the endoplasmic reticulum as a gain-of-toxic function of the mutant protein.[2] Excessive PLP1 protein resulting from genomic duplications may accumulate in late endosomes/lysosomes, promoting its incorporation into other myelin components.[1] In contrast, patients with *PLP1* null mutations escape severe impairments because of the absence of any gain-of-toxic function.[2,13,17] Indeed, knockout mice with a functionally null *Plp1* gene do not develop classical signs of *Plp1*-related disease; their oligodendrocytes develop normally and synthesize compact myelin sheaths.[3,18] However, the mice show ultrastructural abnormalities, including swelling of the small-diameter axons and late-onset axonal degeneration.[3,19] Consequently, a loss-of-function mutation of *PLP1* does not induce oligodendrocyte cell death, possibly serving as a mechanism underlying the milder phenotypic consequences observed in patients with null *PLP1* mutations. Although length-dependent axonal degeneration has been described in *PLP1* null mutations,[20] there is no information about peripheral neuropathy in Patient 1. Thus, it was unclear whether the clinical condition of Patient 1 is compatible with that of *PLP1* null mutations. However, the lack of *PLP1* expression in iPS cells derived from Patient 1 clearly demonstrated that the underlying mechanism of PMD in Patient 1, with a partial *PLP1* duplication, is different from the other two patients in this study.

Immortalized lymphocytes and skin fibroblasts derived from patients are often used for expression studies or biological analyses, as these cells are easy to be obtained and handled. However, many tissue-specific genes are not sufficiently expressed by these cells; *PLP1* being one of them. Although there are reports examining *PLP1* expression by RT–PCR, using mRNA extracted from skin fibroblasts,[4,5,21] the expression of *PLP1* mRNA in skin fibroblasts is too low to be examined by northern blotting as shown here. In this study, our microarray database search showed over 40 times higher *PLP1* expression in iPS cells than that in skin fibroblasts. Our initial northern blot analysis confirmed faint but detectable *PLP1* expression in iPS cells, whereas no expression was observed in skin fibroblasts, lymphocytes or SNL feeder cells. This study also confirmed a lack of *PLP1* expression in SNL feeder cells. Therefore, this study demonstrates that iPS cells express endogenous *PLP1*, and that the possibility of contamination from SNL feeder cells or original skin fibroblasts can be excluded. Although being detectable by northern blotting, *PLP1* expression in iPS cells appeared to be much lower than that in mature oligodendrocytes and may be simply cryptic rather than functional. If so, this allows us to evaluate the native transcriptional level of each mutant (and wild-type) *PLP1* allele, which is the primary focus of our study. Meanwhile, terminal differentiation of iPS cells into the oligodendrocyte lineage would result in an enhanced *PLP1* expression with functional consequence. However, this requires technological breakthrough in the induction of terminal differentiation into oligodendrocyte lineage, which is currently unavailable.

In conclusion, we identified the first PMD patient having a partial *PLP1* duplication. The absence of *PLP1* expression in iPS cells, generated from the patient's skin fibroblasts, proved the underlying effects of the partial *PLP1* duplication for the PMD development.

CONFLICT OF INTEREST

The authors declare no conflict of interest.

ACKNOWLEDGEMENTS

We thank the patients and their families for their cooperation. This work was mainly supported by JST PRESTO program (KS) and was partially supported by Grant-in-Aid for Scientific Research on Innovated Areas 'Foundation of Synapse and Neurocircuit Pathology' and Grant-in-Aid for scientific research from Health Labor Sciences Research Grants from the Ministry of Health, Labor and Welfare, Japan (TY). This work was supported in part by Grant-in-Aid for Scientific Research (A) 21249062, Japan Society for the Promotion of Science (JSPS) and 'High-Tech Research Center' Project for Private Universities: matching fund subsidy from the Ministry of Education, Culture, Sports, Science and Technology, 2006–2010 'The Research Center for the Molecular Pathomechanisms of Epilepsy, Fukuoka University', Research Grants (21B-5) for Nervous and Mental Disorder from the Ministry of Health, Labor and Welfare and Health and Labor Science Research Grant 21210301, KB220001 from the Ministry of Health, Labor and Welfare, and Adaptable and Seamless Technology Transfer Program through Target-driven R&D (A-STEP) Exploratory Research, Japan Science and Technology Agency (JSP) (SH). KS thanks Hayashi Memorial Foundation for Female Natural Scientists for grant aid support.

WEB SITE: NCBI GEO; http://www.ncbi.nlm.nih.gov/guide/genes-expression/
OMIM; http://omim.org/

1 Inoue, K. PLP1-related inherited dysmyelinating disorders: Pelizaeus-Merzbacher disease and spastic paraplegia type 2. *Neurogenetics* **6,** 1–16 (2005).
2 Garbern, J.Y. Pelizaeus-Merzbacher disease: Genetic and cellular pathogenesis. *Cell. Mol. Life Sci.* **64,** 50–65 (2007).
3 Woodward, K.J. The molecular and cellular defects underlying Pelizaeus-Merzbacher disease. *Expert. Rev. Mol. Med.* **10,** e14 (2008).
4 Hobson, G.M., Huang, Z., Sperle, K., Sistermans, E., Rogan, P.K., Garbern, J.Y. *et al.* Splice-site contribution in alternative splicing of PLP1 and DM20: molecular studies in oligodendrocytes. *Hum. Mutat.* **27,** 69–77 (2006).
5 Regis, S., Grossi, S., Corsolini, F., Biancheri, R. & Filocamo, M. PLP1 gene duplication causes overexpression and alteration of the PLP/DM20 splicing balance in fibroblasts from Pelizaeus-Merzbacher disease patients. *Biochim. Biophys. Acta.* **1792,** 548–554 (2009).
6 Inoue, H. Neurodegenerative disease-specific induced pluripotent stem cell research. *Exp. Cell. Res.* **316,** 2560–2564 (2010).
7 Takahashi, K., Tanabe, K., Ohnuki, M., Narita, M., Ichisaka, T., Tomoda, K. *et al.* Induction of pluripotent stem cells from adult human fibroblasts by defined factors. *Cell* **131,** 861–872 (2007).
8 Shimojima, K., Inoue, T., Hoshino, A., Kakiuchi, S., Watanabe, Y., Sasaki, M. *et al.* Comprehensive genetic analyses of PLP1 in patients with Pelizaeus-Merzbacher disease applied by array-CGH and fiber-FISH analyses identified new mutations and variable sizes of duplications. *Brain Dev.* **32,** 171–179 (2010).
9 Warshawsky, I., Chernova, O.B., Hubner, C.A., Stindl, R., Henneke, M., Gal, A. *et al.* Multiplex ligation-dependent probe amplification for rapid detection of proteolipid protein 1 gene duplications and deletions in affected males and carrier females with Pelizaeus-Merzbacher disease. *Clin. Chem.* **52,** 1267–1275 (2006).
10 Ohnuki, M., Takahashi, K. & Yamanaka, S. Generation and characterization of human induced pluripotent stem cells. *Curr. Protoc. Stem Cell Biol.* Chapter 4, Unit 4A2 (2009).
11 Yamamoto, T., Feng, J.H., Higaki, K., Taniguchi, M., Nanba, E., Ninomiya, H. *et al.* Increased NPC1 mRNA in skin fibroblasts from Niemann-Pick disease type C patients. *Brain Dev.* **26,** 245–250 (2004).
12 Iwaki, A., Muramoto, T., Iwaki, I., Furumi, H., Dario-deLeon, M.L., Tateishi, J. *et al.* A missense mutation in the proteolipid protein gene responsible for Pelizaeus-Merzbacher disease in a Japanese family. *Hum. Mol. Genet.* **2,** 19–22 (1993).
13 Cailloux, F., Gauthier-Barichard, F., Mimault, C., Isabelle, V., Courtois, V., Giraud, G. *et al.* Genotype-phenotype correlation in inherited brain myelination defects due to proteolipid protein gene mutations. Clinical European Network on Brain Dysmyelinating Disease. *Eur. J. Hum. Genet.* **8,** 837–845 (2000).
14 Dhaunchak, A.S. & Nave, K.A. A common mechanism of PLP/DM20 misfolding causes cysteine-mediated endoplasmic reticulum retention in oligodendrocytes and Pelizaeus-Merzbacher disease. *Proc. Natl Acad. Sci. USA* **104,** 17813–17818 (2007).
15 Lee, J.A., Inoue, K., Cheung, S.W., Shaw, C.A., Stankiewicz, P. & Lupski, J.R. Role of genomic architecture in PLP1 duplication causing Pelizaeus-Merzbacher disease. *Hum. Mol. Genet.* **15,** 2250–2265 (2006).
16 Woodward, K.J., Cundall, M., Sperle, K., Sistermans, E.A., Ross, M., Howell, G. *et al.* Heterogeneous duplications in patients with Pelizaeus-Merzbacher disease suggest a mechanism of coupled homologous and nonhomologous recombination. *Am. J. Hum. Genet.* **77,** 966–987 (2005).
17 Sistermans, E.A., de Wijs, I.J., de Coo, R.F., Smit, L.M., Menko, F.H. & van Oost, B.A. A (G-to-A) mutation in the initiation codon of the proteolipid protein gene causing a relatively mild form of Pelizaeus-Merzbacher disease in a Dutch family. *Hum. Genet.* **97,** 337–339 (1996).
18 Klugmann, M., Schwab, M.H., Puhlhofer, A., Schneider, A., Zimmermann, F., Griffiths, I.R. *et al.* Assembly of CNS myelin in the absence of proteolipid protein. *Neuron* **18,** 59–70 (1997).
19 Griffiths, I., Klugmann, M., Anderson, T., Yool, D., Thomson, C., Schwab, M.H. *et al.* Axonal swellings and degeneration in mice lacking the major proteolipid of myelin. *Science* **280,** 1610–1613 (1998).
20 Garbern, J.Y., Yool, D.A., Moore, G.J., Wilds, I.B., Faulk, M.W., Klugmann, M. *et al.* Patients lacking the major CNS myelin protein, proteolipid protein 1, develop length-dependent axonal degeneration in the absence of demyelination and inflammation. *Brain* **125,** 551–561 (2002).
21 Mikesova, E., Barankova, L., Sakmaryova, I., Tatarkova, I. & Seeman, P. Quantitative multiplex real-time PCR for detection of PLP1 gene duplications in Pelizaeus-Merzbacher patients. *Genet. Test.* **10,** 215–220 (2006).

Supplementary Information accompanies the paper on Journal of Human Genetics website (http://www.nature.com/jhg)

European Journal of Medical Genetics 55 (2012) 400–403

Contents lists available at SciVerse ScienceDirect

European Journal of Medical Genetics

journal homepage: http://www.elsevier.com/locate/ejmg

Short clinical report

Pelizaeus-Merzbacher disease caused by a duplication-inverted triplication-duplication in chromosomal segments including the *PLP1* region

Keiko Shimojima [a], Toshiyuki Mano [b], Mitsuru Kashiwagi [c], Takuya Tanabe [d], Midori Sugawara [a], Nobuhiko Okamoto [e], Hiroshi Arai [f], Toshiyuki Yamamoto [a,*]

[a] *Tokyo Women's Medical University Institute for Integrated Medical Sciences, Tokyo, Japan*
[b] *Department of Pediatric Neurology, Osaka Medical Center and Research Institute for Maternal and Child Health, Osaka, Japan*
[c] *Division of Pediatrics, Hirakata City Hospital, Hirakata, Japan*
[d] *Department of Pediatric Neurology, Tanabe-Kadobayashi Children's Clinic, Hirakata, Japan*
[e] *Department of Medical Genetics, Osaka Medical Center and Research Institute for Maternal and Child Health, Osaka, Japan*
[f] *Department of Pediatric Neurology, Morinomiya Hospital, Osaka, Japan*

ARTICLE INFO

Article history:
Received 28 September 2011
Accepted 29 February 2012
Available online 21 March 2012

Keywords:
Pelizaeus-Merzbacher disease (PMD)
Proteolipid protein 1 (*PLP1*)
Microarray-based comparative genomic hybridization (aCGH)
Fluorescence *in situ* hybridization (FISH)
Triplication
DUP-TRP/INV-DUP

ABSTRACT

Pelizaeus-Merzbacher disease (PMD; MIM#312080) is a rare X-linked leukodystrophy presenting with motor developmental delay associated with spasticity and nystagmus. PMD is mainly caused by abnormalities in the proteolipid protein 1 gene (*PLP1*), most frequently due to duplications of chromosomal segments including *PLP1*. In this study, a 9-year-old male patient manifesting severe developmental delay and spasticity was analyzed for *PLP1* alteration, and triplication of *PLP1* was identified. Further examination revealed an underlying genomic organization, duplication-inverted triplication-duplication (DUP-TRP/INV-DUP), in which a triplicated segment was nested between 2 junctions. One of the 2 junctions was caused by inverted homologous regions, and the other was caused by non-homologous end-joining. PMD patients with *PLP1* duplications usually show milder-classical forms of the disease compared with patients with *PLP1* missense mutations manifesting severe connatal forms. The present patient showed severe phenotypic features that represent an intermediate form of PMD between classical and connatal forms. This is the first report of a patient with *PLP1* triplication caused by a DUP-TRP/INV-DUP structure. This study adds additional evidence about the consequences of *PLP1* triplication.

1. Introduction

Pelizaeus-Merzbacher disease (PMD; MIM#312080) is a rare X-linked leukodystrophy presenting with nystagmus, hypotonia that later develops into spasticity, dystonia, ataxia, and developmental delay beginning in the first year of life [4,9]. The proteolipid protein 1 gene (*PLP1*; MIM#300401) is the main responsible gene for PMD and the most common *PLP1* alterations are gene duplications, which are found in 60–70% of PMD patients [4,9]. Nucleotide alterations that affect the amino acid sequences of *PLP1* are found in 20% of PMD patients. The clinical manifestations of patients with *PLP1* alterations are dependent on the genotypes.

Recently, we identified a rare *PLP1* triplication in a patient with PMD. In this study, we revealed the underlying genomic organization with a duplication-inverted triplication-duplication (DUP-TRP/INV-DUP), which is a recently proposed mechanism of chromosomal rearrangement [2]. The clinical implication of *PLP1* gene dosage effects is discussed.

2. Materials, methods, and results

2.1. Clinical report

A 9-year-and-10-month-old boy was born at 38 weeks of gestation with a birth weight of 2400 g. Although his siblings were healthy, his maternal uncle and male cousin showed similar manifestations as his own; his maternal male cousin died at the age of 7 years (Supplemental Fig. S1). After birth, he showed nystagmus, laryngeal stridor, and profound hypotonia, and his subsequent psychomotor development was severely delayed. At the age of 5 months, his brain magnetic resonance imaging (MRI)

* Corresponding author.
E-mail addresses: toshiyukiyamamoto@twmu.ac.jp, yamamoto@imcir.twmu.ac.jp (T. Yamamoto).

1769-7212/$ – see front matter © 2012 Elsevier Masson SAS. All rights reserved.
doi:10.1016/j.ejmg.2012.02.013

revealed hypomyelination, which became profound at the age of 5 years and 5 months (Fig. 1).

At present, his height is 108 cm (<3rd centile), weight is 13.0 kg (<3rd centile), and head circumference is 47.7 cm (<3rd centile), indicating microcephaly. He shows severe developmental delay. He cannot turn over or sit on his own. Although he shows a lack of stable head control, he does not require head support when sitting in a "chair" position. He can eat minced food orally but with full support. Toilet habit is not acquired. He can vocalize, although very slowly, and can show his intentions by using simple signs or buttons. Mild scoliosis and mildly restricted range of movement in his hip and knee joints are noted. Neurological examination reveals mild muscular hypotonia. Pyramidal tract signs are prominent in his lower extremities; decreased deep tendon reflexes in his upper extremities, diminished abdominal reflex, increased deep tendon reflexes in his lower extremities, and positive Babinski reflex and ankle clonus in both his legs are also noted. Although some cerebellar signs are positive with continuous horizontal nystagmus and trunkal ataxia, the other findings are negative, including intention tremor and dysmetria. No dystonic finding is noted. Because he has never shown epileptic seizures, he has never been evaluated with electroencephalography. Moreover, no nerve conduction velocity tests have been done.

2.2. Cytogenetic analysis

From his clinical features, PMD was suspected as the candidate diagnosis. Then, we analyzed *PLP1* gene dosage by multiplex ligation-dependent probe amplification (MLPA) analysis, using Holland SALSA P022 MLPA probe mix (MRC Holland, Amsterdam, the Netherlands) according to the manufacturer's protocol [7]. The peak height of *PLP1* in this patient was higher than that of previously evaluated patients with *PLP1* duplication, which led us to suspect triplication of *PLP1* rather than duplication (data not shown). To confirm this MLPA result, microarray-based comparative genomic hybridization (aCGH) analysis was performed using the Agilent catalog 105K oligonucleotide microarray (Agilent Technologies, Santa Clara, CA) according to the method described elsewhere [6], and the chromosomal aberration region was revealed to consist of duplicated and triplicated regions. To identify the precise aberration regions, a custom-made oligoarray was originally designed using the web-based software Agilent earray (https://earray.chem.agilent.com/earray/), according to the manufacturer's protocol. The array included 11,526 probes between chrX 101,600,412–103,499,946 with an average interval of 147-bp (Agilent Technologies). Finally, genomic copy number gain was identified on Xq22.2 with a size of 984-kb (chrX: 102,321,416–103,305,265) in which a nested aberration of 214-kb including *PLP1* (chrX: 103,010,204–103,223,711) was included (Fig. 2A, Table 1).

The identified aberration was further examined by fluorescence *in situ* hybridization (FISH) as previously described [6]. Metaphase and interphase nuclei were prepared from peripheral blood lymphocyte-stimulated phytohemagglutinin according to the standard method. Human bacterial artificial clones were selected from the UCSC Genome Browser (http://www.genome.ucsc.edu) as described previously [6]. The results of FISH analysis were compatible with that of aCGH and confirmed that the triplicated region including *PLP1* was surrounded by duplicated regions (Fig. 2B–D). The patient's mother declined examination for the carrier status of *PLP1* triplication.

The underlying genomic organization was investigated using long range PCR-based analyses with Tks Gflex™ DNA Polymerase (Takara, Ohtsu, Japan). The primers used for PCR are listed in Supplemental Table S1. The combinatory use of sense primers A and B generated an appropriately 20-kb PCR product, which fit the predicted architecture of junction 1 (Fig. 3A and B). The combinatory use of antisense primers C and D also generated a 756-bp PCR product (Fig. 3A and B). Direct sequencing analysis identified the junction 2 sequence (Fig. 3C). Because there is no homologous sequence in junction 2, this rearrangement was considered a consequence of non-homologous end-joining (NHEJ) [4].

3. Discussion

We presented a male patient with generalized spasticity, severe developmental delay, and hypomyelination. His condition was diagnosed as PMD on the basis of clinical findings. We detected *PLP1* triplication from combined examinations with MLPA, aCGH, and FISH analyses. aCGH analysis confirmed a duplicated region on Xq22.2 in which a nested aberration with triplicated region of *PLP1* was identified.

Recently, Carvalho et al. proposed a new mechanism for genomic rearrangement causing the genomic organization DUP-TRP/INV-DUP in 5 patients with *MECP2*-related disorders [2], in whom various sizes of triplicated segments were found embedded in the neighboring duplicated segments and were inserted in an inverted orientation. The existence of inverted repeats in the

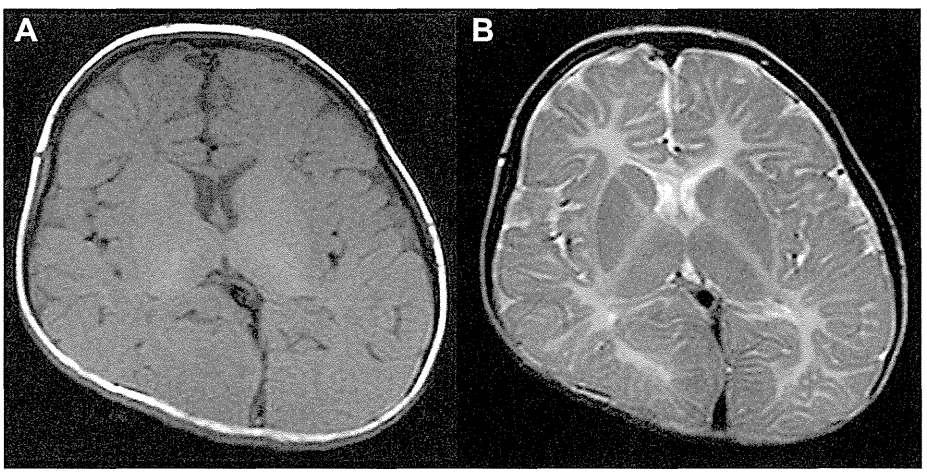

Fig. 1. Brain MRI of the patient performed at 5 years and 5 months of age. The reduction in the contrast of cortex and white matter in T1-weighted image (A) and the diffuse hypersignal in T2-weighted image (B) show severe hypomyelination. Complete lack of myelination is also shown in the posterior limb of internal capsule.

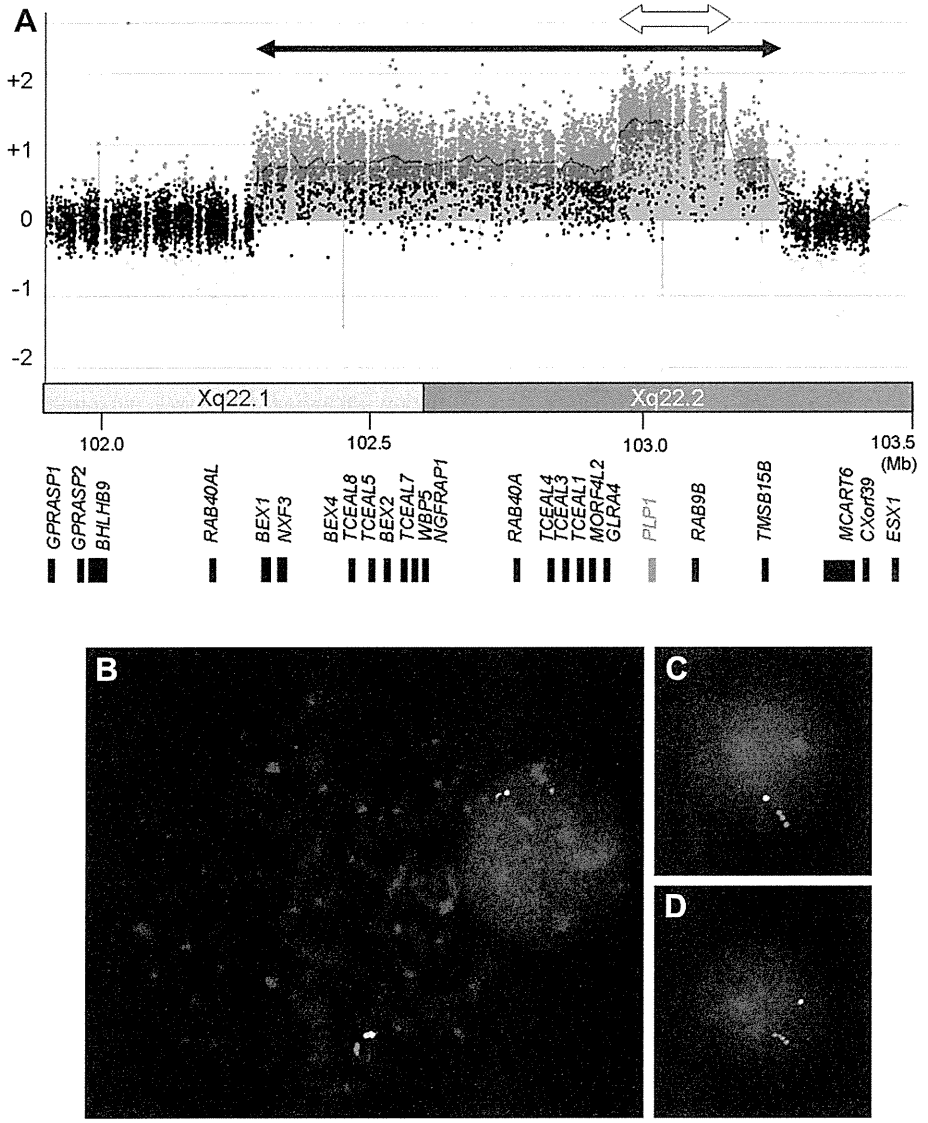

Fig. 2. Results of cytogenetic and molecular analyses. (A) The genome view of the result of custom array represents a chromosomal duplication (black bar with arrow on both ends) and a nested triplication including *PLP1* (white bar with arrow on both ends). (B) Two green signals of CTD-2086O16 (chrXq22.2: 102,807,623–102,897,468) were identified in the interphase nuclei, indicating duplication of this region. The red signal of RP11-75D20 (chrXp22.13: 18,314,474–18,506,931) was used as a marker. Both of the signals are on the same X chromosome, indicating that the *PLP1* locus is not translocated on the other chromosome. (C, D) Three red signals of RP4-540A13 (chrXq22.2: 103,067,273–10,3152,647) were identified in the interphase nuclei, indicating triplication of this region. The green signal of RP11-106N3 (chrXp22.13: 18,467,339–18,626,601) was used as a marker.

telomeric side mediates these inverted rearrangements [2]. Although the authors also identified a DUP-TRP/INV-DUP structure in the neighboring region of *PLP1* in one individual, the triplicated region did not include *PLP1* itself. In this study, we identified a DUP-TRP/INV-DUP structure in the present patient with PMD, and *PLP1* was included in the triplicated region. Detailed molecular examination revealed that two H2B histone family member X pseudogenes, *H2BFXP*, were located at each of the telomeric ends of the triplication and duplication (Fig. 3A). According to the UCSC Genome Browser, the two *H2BFXP* showed 99% identical sequences and were inserted in an inverted orientation (Fig. 3A). The result of this study indicated that the inverted orientation of *H2BFXP* mediated the first rearrangement (junction 1), and this caused the insertion of an inverted segment including *PLP1* and resulted as the triplication of this region. The 2nd rearrangement was caused by NHEJ [4], because there was no homologous sequence in junction 2 (Fig. 3C). From these results, the mechanism of the chromosomal

Table 1

The summary of the genomic copy number aberration

Chromosome band		Position	Average $\log_2$ ratio	Locus	
chrX		102,320,921			
	q22.1	102,321,416	Duplication		Primer D
		102,807,623	0.76	CTD-2086O16	
		102,897,468			
		103,009,875			
		103,010,204	Triplication		Primer C
		103,031,781	1.25	*PLP1*	
		103,047,545			
	q22.2	103,067,273		RP4-540A13	
		103,152,647			
		103,223,711			Primer A
				H2BFXP	
		103,243,004			
		103,305,265			
				H2BFXP	
		103,328,529			Primer B

Genomic position is reffered to build 19

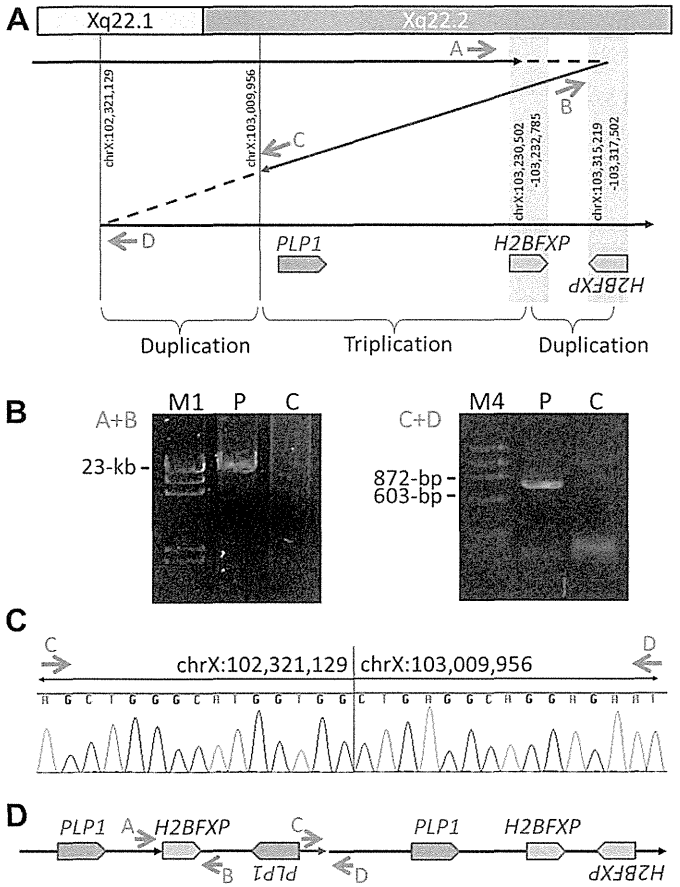

Fig. 3. Genomic organization of the present patient. (A) Predicted chromosomal rearrangements around Xq22.2. Red arrows, locations and directions of primers; trapezoids, locations and directions of genes; blue arrow, inverted genomic region. (B) Results of the electropherogram of the PCR products. The combinatory use of primers A + B generated an approximately 20-kb PCR product of junction 1, and primers C + D generated a 756-bp PCR product. M1, molecular marker of λ/*Hind*III digest; M4, molecular marker of φX175/HaeIII digest; P, the present patient; C, normal control. (C) The sequencing electropherogram indicates junction 2, generated by PCR using primers C + D. (D) The final conclusion about the genomic organization is shown in the horizontal view.

rearrangement identified in this study can be explained by DUP-TRP/INV-DUP (Fig. 3D) [2].

Traditionally, PMD was classified into 3 categories: connatal form, classical form, and X-linked spastic paraplegia type 2 (SPG2; MIM#312920) [4]. Callioux et al. proposed a new subclassification of PMD as a continuous clinical spectrum [1]. According to these 2 classification systems, PMD patients with simple *PLP1* duplications manifest rather milder phenotypes (classical form/form 1–2), whereas PMD patients with nucleotide alterations often show severe phenotypes (connatal form/form 0). As the present patient has never achieved head control, his clinical condition can be traditionally classified as the connatal type and regarded as form 0 according to Callioux et al.'s classification [1]. However, he can eat minced food orally and there is no strider at present. Thus, we regarded his condition as an intermediate form of PMD between classical (form 1) and connatal (form 0).

There have been only few reports of PMD patients with more than 2 copies of *PLP1* [3,5,8]. Five male patients with *PLP1* triplication reported by Wolf et al. showed severe clinical features compared with patients with *PLP1* duplications [8]. None of the 5 patients achieved stable head control, and their brain MRI showed an almost complete absence of the normal myelin signal [8]. The present patient also showed lack of stable head control, severe mental retardation, and a complete lack of myelination in the posterior limb of internal capsule was identified by brain MRI. Thus, our study gives evidence that patients with *PLP1* triplications show a more severe phenotype than patients with *PLP1* duplications.

Conflict of interest

The authors declare no conflict of interests.

Acknowledgements

This work was supported by Health Labor Sciences Research Grants from the Ministry of Health, Labor, and Welfare, Japan.

Appendix A. Supplementary data

Supplementary data associated with this article can be found, in the online version, at doi:10.1016/j.ejmg.2012.02.013.

References

[1] F. Cailloux, F. Gauthier-Barichard, C. Mimault, V. Isabelle, V. Courtois, et al., Genotype-phenotype correlation in inherited brain myelination defects due to proteolipid protein gene mutations. Clinical European Network on brain dysmyelinating disease, Eur. J. Hum. Genet. 8 (2000) 837–845.
[2] C.M. Carvalho, M.B. Ramocki, D. Pehlivan, L.M. Franco, C. Gonzaga-Jauregui, et al., Inverted genomic segments and complex triplication rearrangements are mediated by inverted repeats in the human genome, Nat. Genet. 43 (2011) 1074–1081.
[3] P. Combes, M.N. Bonnet-Dupeyron, F. Gauthier-Barichard, R. Schiffmann, E. Bertini, et al., PLP1 and GPM6B intragenic copy number analysis by MAPH in 262 patients with hypomyelinating leukodystrophies: identification of one partial triplication and two partial deletions of PLP1, Neurogenetics 7 (2006) 31–37.
[4] K. Inoue, PLP1-related inherited dysmyelinating disorders: Pelizaeus-Merzbacher disease and spastic paraplegia type 2, Neurogenetics 6 (2005) 1–16.
[5] J.A. Lee, C.M. Carvalho, J.R. Lupski, A DNA replication mechanism for generating nonrecurrent rearrangements associated with genomic disorders, Cell 131 (2007) 1235–1247.
[6] K. Shimojima, T. Inoue, A. Hoshino, S. Kakiuchi, Y. Watanabe, et al., Comprehensive genetic analyses of PLP1 in patients with Pelizaeus-Merzbacher disease applied by array-CGH and fiber-FISH analyses identified new mutations and variable sizes of duplications, Brain Dev. 32 (2010) 171–179.
[7] I. Warshawsky, O.B. Chernova, C.A. Hubner, R. Stindl, M. Henneke, et al., Multiplex ligation-dependent probe amplification for rapid detection of proteolipid protein 1 gene duplications and deletions in affected males and carrier females with Pelizaeus-Merzbacher disease, Clin. Chem. 52 (2006) 1267–1275.
[8] N.I. Wolf, E.A. Sistermans, M. Cundall, G.M. Hobson, A.P. Davis-Williams, et al., Three or more copies of the proteolipid protein gene PLP1 cause severe Pelizaeus-Merzbacher disease, Brain 128 (2005) 743–751.
[9] K.J. Woodward, The molecular and cellular defects underlying Pelizaeus-Merzbacher disease, Expert Rev. Mol. Med. 10 (2008) e14.

ELSEVIER

Brain & Development 36 (2014) 57–60

BRAIN & DEVELOPMENT
Official Journal of the Japanese Society of Child Neurology

www.elsevier.com/locate/braindev

Case report

MR spectroscopy in 18q⁻ syndrome suggesting other than hypomyelination

Hiroko Tada [a,*], Jun-ichi Takanashi [b,c]

[a] *Department of Pediatrics, Chibaken Saiseikai Narashino Hospital, Narashino, Japan*
[b] *Department of Pediatrics, Kameda Medical Center, Kamogawa, Japan*
[c] *Department of Radiology, Toho University Sakura Medical Center, Sakura, Japan*

Received 12 July 2012; received in revised form 17 September 2012; accepted 6 December 2012

Abstract

We reported a 5-year-old boy with 18q⁻ syndrome who showed typical magnetic resonance imaging (MRI) findings of high signal intensity on T2-weighted imaging, and a slightly high but lower than normal signal on T1-weighted imaging of the white matter. MR spectroscopy (MRS) revealed increased concentrations of creatine, myoinositol and choline with a normal *N*-acetylaspartate one. The cerebral white matter lesions observed on MRI in patients with 18q⁻ syndrome have been considered to reflect hypomyelination due to a decrease in myelin basic protein so far, however, MRS suggested reactive astrocytic gliosis and accelerated myelin turnover, which are compatible with recent pathological reports of 18q⁻ syndrome.

Keywords: 18q⁻ syndrome, MR spectroscopy; Hypomyelination; Gliosis; *MBP* gene

1. Introduction

18q⁻ syndrome is a rare chromosomal disorder involving frequent abnormal intensity of the white matter on T2-weighted imaging (T2WI) and the following clinical features: developmental delay, growth retardation, hearing loss, hypotonia, craniofacial dysmorphism, foot deformities, and eye movement disorders. Myelin basic protein (MBP) accounts for 30–40% of the total myelin protein in the central nervous system [1], and is thought to play an important role in myelin compaction. As the gene for MBP is encoded on 18q23, the region most commonly deleted in 18q⁻ syndrome [2,3], it has been considered that the magnetic resonance imaging (MRI) findings probably reflect hypomyelination due to a haploinsufficiency of MBP [1]. We report a 5-year-old boy with 18q⁻ syndrome in whom quantitative MR spectroscopy (MRS) revealed increased choline (Cho), creatine (Cr), and myoinositol (mIns) concentrations. The increased Cho suggested accelerated myelin turnover rather than hypomyelination, and the increased Cr and mIns suggested astrocytic gliosis. The latter is compatible with a recent neuropathological report of 18q⁻ syndrome.

2. Case report

The patient, a 5-year-old Japanese boy, was delivered at 40 weeks gestation by means of vacuum extraction, weighing 3656 gm. He had no congenital cardiac disease or hearing loss. His motor and mental development were slow; he could only roll over at 6 months, sit alone at 9 months, and walk with support at 15 months and without support at 23 months. He did not utter any significant words at 2 years. G-Banding analysis revealed

* Corresponding author. Address: Department of Pediatrics, Chibaken Saiseikai Narashino Hospital, 1-1-1, Izumi-cho, Narashino City, Chiba 275-8580, Japan. Fax: +81 47 478 6601.
E-mail address: h.tada@hotmail.co.jp (H. Tada).

0387-7604/$ - see front matter
http://dx.doi.org/10.1016/j.braindev.2012.12.003

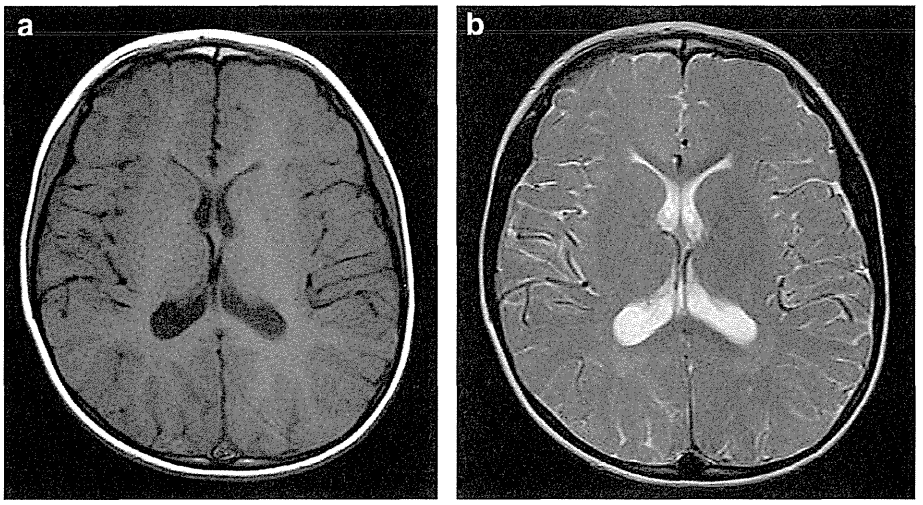

Fig. 1. (a) T1-weighted image showing the white matter exhibited higher intensity than the gray matter, but it was still lower than normal. (b) T2-weighted image showing the slightly high intensity in other white matter regions with poor gray and white matter contrast.

Table 1
Concentrations of metabolites (mM) determined with an LCModel in 18q$^-$ syndrome.

	ROI	NAA	Cr	Cho	mIns
18q$^-$ syndrome	WM	7.66	4.76	1.72	4.26
Normal	WM	6.87 ± 0.59	3.59 ± 0.33	1.25 ± 0.11	3.13 ± 0.51

NAA, *N*-acetylaspartate; Cr, creatine; Cho, choline; mIns, myoinositole; ROI, region of interest; WM, white matter.

46, XY, del (18) (q21.3), leading to a diagnosis of 18q$^-$ syndrome. His developmental questionnaire score was 46 at 5 years. He also presented with a short stature and craniofacial dysmorphism, such as a prominent forehead, brachycephaly, narrow eye clefts, hypertelorism, midface hypoplasia, epicanthal folds, a small upturned nose, and a carp-like mouth.

At 5 years, T1WI, T2WI and MRS (PRESS TR/TE = 5000/30) were performed with a 1.5 T Siemens apparatus. The concentrations of metabolites were quantitated with an LCModel using the modified water scaling method as previously reported [4]. On T1WI, the white matter exhibited slightly higher intensity than the gray matter, but it was still lower than normal (Fig. 1). T2WI showed low intensity in the corpus callosum, but slightly high intensity in the other white matter regions with poor gray and white matter contrast (Fig. 1). MRS revealed increased concentrations of Cho, Cr and mIns with a normal *N*-acetylaspartate (NAA) (Table 1 and Fig. 2).

3. Discussion

This is the first report of increased Cho observable on MRS in a patient with 18q$^-$ syndrome, suggesting the underlying pathology is other than hypomyelination with reduced Cho. MR-visible Cho is derived from various cell membrane precursors and breakdown products, such as phosphocholine, glycerophosphocholine, and phosphatidylcholine, reflecting myelin metabolism, therefore, the Cho level increases during the newborn period, when myelin sheaths are actively being formed [5,6], and the acute phase of demyelination. MRS in patients with Pelizaeus-Merzbacher disease (PMD), a representative hypomyelination disorder, shows decreased Cho reflecting hypomyelination, that is, an absence of myelin and mature oligodendrocytes [5,6]. On the other hand, a recent neuropathological study on a patient with 18q$^-$ syndrome revealed prominent astrogliosis, and normal myelinated fibers were observed on microscopical examination, which is distinct from in PMD. Immunohistological examination revealed normal immunoreactivity for MBP in myelinated fibers, but reduced immunoreactivity in oligodendrocytes [7]. Some functional abnormalities of oligodendrocytes may result in the increased myelin turnover and increase in Cho observable on MRS.

Shiverer mice with an abnormal *mbp* gene (*mbp* −/−) showed little or no myelination in a neuropathological study, and diffuse T2 prolongation in the white matter on MRI [8]. On the other hand, heterozygous mice (*mbp* +/−) show normal myelin sheaths and normal MRI findings [8], despite the presence of only half the normal amount of mbp protein. The heterozygous mice also show no clinical symptoms, however, the visually evoked potential (VEP) latency has been reported to

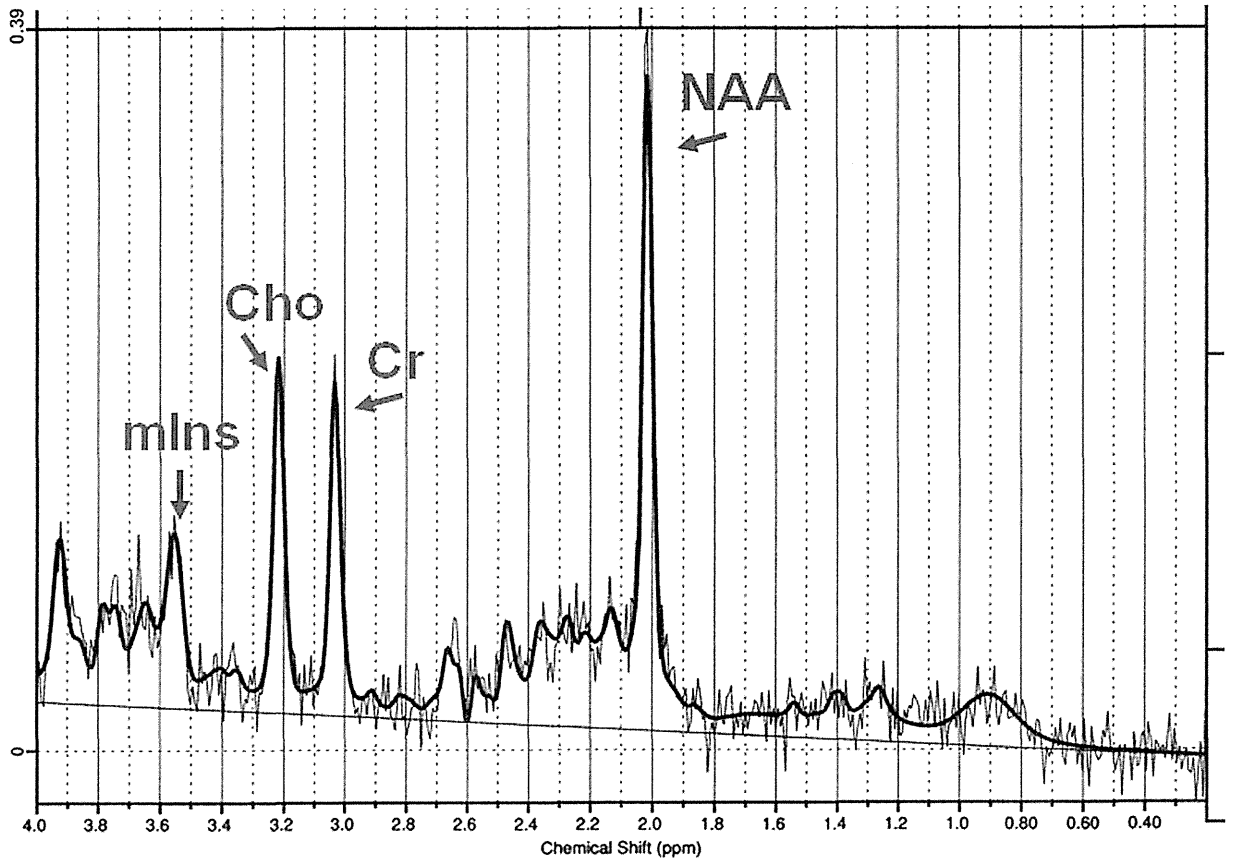

Fig. 2. MRS of the left white matter showing elevated Cho, Cr and mIns.

be increased [8], suggesting a dysfunction of the optic nerves. This might support our hypothesis for 18q$^-$ syndrome that a dysfunction of oligodendrocytes and myelinated fibers may result in increased turnover of myelin and increased Cho. MRS of heterozygous mice (*mbp* +/−) would allow more accurate assessment of the hypothesis.

Increased mIns, which is abundant in astrocytes, is considered to reflect astrogliosis [5,6]. Cr is more concentrated in glia than in neurons, and is also expected to be increased in astrogliosis [5]. Increases in Cr and mIns in 18q$^-$ syndrome would, therefore, reflect astrogliosis, as shown by a recent pathological study [7]. We speculate that the astrogliosis results in T2 prolongation in the white matter. Because heterozygous mice show no astrogliosis (unpublished data), it is speculated that a broad gene deletion in patients with 18q$^-$ syndrome includes not only the *MBP* gene, but also another gene or genes causing astrogliosis, that is, 18q$^-$ syndrome is a contiguous gene syndrome.

To our knowledge, there has been only one report of MRS in a patient with 18q$^-$ syndrome, which showed increased Cho/Cr at 30-months-old, followed by a decrease in it during follow-up [9].Because the Cr concentrations remains relatively constant in the brain in different metabolic conditions, it is often used as a reference to measure NAA and Cho, however, altered concentrations of Cr have been reported [4], as observed in this patient. Therefore, normalizing the Cho value as to Cr would be inappropriate and lead to misunderstanding of the results, especially when both are increased. To resolve this problem, we performed absolute quantification of the metabolite with an LCModel, which confirmed the increased concentration of Cho.

In conclusion, the results of MRS in a patient with 18q$^-$ syndrome suggest increased myelin turnover and gliosis, and not the hypomyelination previously considered.

Acknowledgements

This study was supported in part by a Grant-in-aid for Research on Measures for Intractable Diseases (H24-Nanchi-Ippan-72), and a Research Grant for Nervous and Mental Disorders (24-7), both from the Ministry of Health, Labor and Welfare of Japan; and by a Grant-in-Aid for Scientific Research (C-24591790) from the Japan Society for the Promotion of Science.

References

[1] van der Knaap MS, Valk J. 18q$^-$ syndrome. In: van der Knaap MS, Valk J, editors. Magnetic resonance of myelination and myelin disorders. Hidelberg, Germany: Springer; 2005. p. 281–3.

[2] Gay CT, Hardies LJ, Rauch RA, Lancaster JL, Plaetke R, DuPont BR, et al. Magnetic resonance imaging demonstrates incomplete myelination in 18q$^-$ syndrome: evidence for myelin basic protein haploinsufficiency. Am J Med Genet 1997;74:422–31.
[3] Hale DE, Cody JD, Baillargeon J, Schaub R, Danney MM, Leach RJ, et al. The spectrum of growth abnormalities in children with 18q deletions. J Clin Endocrinol Metab 2000;85:4450–4.
[4] Takanashi J, Somazawa F, Maruyama K, Terada H, Xu D, Barkovich AJ. Metabolic changes in early childhood using LCModel with corrected water scaling method. J Magn Reson Imaging 2012;35:174–80.
[5] Takanashi J, Saito S, Aoki I, Barkovich AJ, Ito Y, Inoue K. Increased *N*-acetylaspartate in model mouse of Pelizaeus-Merzbacher disease. J Magn Reson Imaging 2012;35:418–25.
[6] Takanashi J, Inoue K, Tomita M, Kurihara A, Morita F, Ikehira H, et al. Brain *N*-acetylaspartate is elevated in Pelizaeus-Merzbacher disease with PLP1 duplication. Neurology 2002;58:237–41.
[7] Tanaka R, Iwasaki N, Hayashi M, Nakayama J, Ohto T, Takahashi M, et al. Abnormal brain MRI signal in 18q$^-$ syndrome not due to dysmyelination. Brain Dev 2012;34:234–7.
[8] Martin M, Hiltner TD, Wood JC, Fraser SE, Jacobs RE, Readhead C. Myelin deficiencies visualized in vivo: visually evoked potentials and T2-weighted magnetic resonance images of shiverer mutant and wild-type mice. J Neurosci Res 2006;84:1716–26.
[9] Häusler M, Anhuf D, Schüler H, Ramaekers VT, Thron A, Zerres K, et al. White-matter disease in 18q deletion (18q$^-$) syndrome: magnetic resonance spectroscopy indicates demyelination or increased myelin turnover rather than dysmyelination. Neuroradiology 2005;47:83–6.

THE JOURNAL OF BIOLOGICAL CHEMISTRY VOL. 288, NO. 11, pp. 7451–7466, March 15, 2013

Depletion of Molecular Chaperones from the Endoplasmic Reticulum and Fragmentation of the Golgi Apparatus Associated with Pathogenesis in Pelizaeus-Merzbacher Disease*

Received for publication, November 13, 2012, and in revised form, January 23, 2013 Published, JBC Papers in Press, January 23, 2013, DOI 10.1074/jbc.M112.435388

Yurika Numata[‡§], Toshifumi Morimura[‡¶], Shoko Nakamura[‡], Eriko Hirano[‡], Shigeo Kure[§], Yu-ich Goto[‡], and Ken Inoue[‡1]

From the [‡]Department of Mental Retardation and Birth Defect Research, National Institute of Neuroscience, National Center of Neurology and Psychiatry (NCNP), 4-1-1 Ogawahigashi-machi, Kodaira-shi, Tokyo 187-8502, the [§]Department of Pediatrics, Tohoku University School of Medicine, 1-1 Seiryomachi, Aobaku, Sendai 980-8574, and the [¶]Unit for Neurobiology and Therapeutics, Molecular Neuroscience Research Center, Shiga University of Medical Science, Seta-Tsukinowa-cho, Otsu, Shiga 520-2192, Japan

Background: Mutations of proteolipid protein 1 (*PLP1*) induce endoplasmic reticulum (ER) stress.
Results: PLP1 mutants deplete some chaperones from the ER and induce fragmentation of the Golgi apparatus (GA).
Conclusion: These changes affect clinical pathology in disease-causing mutations of *PLP1*.
Significance: This work provides a novel insight involving global changes of organelles in pathogenesis of ER stress-related diseases.

Missense mutations in the proteolipid protein 1 (*PLP1*) gene cause a wide spectrum of hypomyelinating disorders, from mild spastic paraplegia type 2 to severe Pelizaeus-Merzbacher disease (PMD). Mutant PLP1 accumulates in the endoplasmic reticulum (ER) and induces ER stress. However, the link between the clinical severity of PMD and the cellular response induced by mutant PLP1 remains largely unknown. Accumulation of misfolded proteins in the ER generally leads to up-regulation of ER chaperones to alleviate ER stress. Here, we found that expression of the PLP1-A243V mutant, which causes severe disease, depletes some ER chaperones with a KDEL (Lys-Asp-Glu-Leu) motif, in HeLa cells, MO3.13 oligodendrocytic cells, and primary oligodendrocytes. The same PLP1 mutant also induces fragmentation of the Golgi apparatus (GA). These organelle changes are less prominent in cells with milder disease-associated PLP1 mutants. Similar changes are also observed in cells expressing another disease-causing gene that triggers ER stress, as well as in cells treated with brefeldin A, which induces ER stress and GA fragmentation by inhibiting GA to ER trafficking. We also found that mutant PLP1 disturbs localization of the KDEL receptor, which transports the chaperones with the KDEL motif from the GA to the ER. These data show that PLP1 mutants inhibit GA to ER trafficking, which reduces the supply of ER chaperones and induces GA fragmentation. We propose that depletion of ER chaperones and GA fragmentation induced by mutant misfolded proteins contribute to the pathogenesis of inherited ER stress-related diseases and affect the disease severity.

A number of inherited human diseases are caused by missense mutations. These mutations in the membrane and secretary proteins often lead to improper protein folding and accumulation in the endoplasmic reticulum (ER),[2] resulting in an induction of ER stress. In cells under ER stress, accumulation of mutant proteins in the ER activates the unfolded protein response (UPR), which initiates a block in translation, increases retrotranslocation and degradation of ER-localized proteins, and bolsters the protein-folding capacity of the ER (1, 2). Through these processes, the UPR functions as a cellular quality control system that essentially protects cells from the toxicity of accumulated proteins in the ER. The UPR is activated by three distinct pathways, activating transcription factor 6 (ATF6), inositol-requiring kinase 1 (IRE1), and protein kinase-like ER kinase (3), all of which are negatively regulated by interaction with the 78-kDa glucose-regulated protein (GRP78, also referred to as BiP/HSPA5). On accumulation of unfolded protein, GRP78 binds to unfolded proteins and dissociates from

* This work was supported in part by grants from the Health and Labor Sciences Research Grants, Research on Intractable Diseases H24-Nanchitou-Ippan-072 (to K. I.), a grant from Takeda Science Foundation (to K. I.), and Grants-in-Aid for Scientific Research from the Ministry of Education, Culture, Sports, Science and Technology, Japan, KAKENHI: 21390103 and 23659531 (to K. I.) and 23580417 (to T. M.).
[1] To whom correspondence should be addressed. Tel.: 81-42-346-1713; Fax: 81-42-346-1743; E-mail: kinoue@ncnp.go.jp.

[2] The abbreviations used are: ER, endoplasmic reticulum; PLP1, proteolipid protein 1; PMD, Pelizaeus-Merzbacher disease; msd, myelin synthesis deficit; SPG2, spastic paraplegia type 2; msd, myelin synthesis deficit; GA, Golgi apparatus; PDI, protein-disulfide isomerase; CALR, calreticulin; GRP78, glucose-regulated protein of 78 kDa; CANX, calnexin; MBP, myelin basic protein; UPR, unfolded protein response; ATF6, activating transcription factor 6; IRE1, inositol-requiring kinase 1; XBP1, X-box protein 1; CHOP, C/EBP homologous protein; ALS, amyotrophic lateral sclerosis; MPZ, myelin protein zero; PMP22, peripheral myelin protein 22; CMT, Charcot-Marie-Tooth disease; SC, spinal cords; TUNEL, terminal deoxynucleotidyl transferase dUTP nick end labeling; MGC, mixed glial culture; BFA, brefeldin A; MOG, myelin oligodendrocyte glycoprotein; GFP, green fluorescent protein; luc, luciferase; Rluc, *Renilla* luciferase; Igκ, immunoglobulin κ light chain; Cluc, cytoplasmic luciferase; DMSO, dimethyl sulfoxide.

the ER stress sensors, which trigger the UPR (3). ATF6 induces transcription of major ER chaperones and X box-binding protein 1 (*XBP1*) (4). The endonuclease activity of IRE1 splices *XBP1* (5), which functions as a transcription factor that drives the expression of UPR-related genes (4). The ATF6 and IRE1-XBP1 axes promote the expression of ER chaperones that facilitate the correct folding or assembly of ER proteins and prevent their aggregation, thereby improving cell survival (3, 4, 6). However, when ER stress overwhelms the capacity of this intrinsic quality control, apoptosis is induced by up-regulation of the C/EBP homologous protein (CHOP).

In inherited diseases associated with ER stress, different mutations in the causative genes result in various phenotypes. One representative example, Pelizaeus-Merzbacher disease (PMD), is an X-linked recessive leukodystrophy characterized by diffuse hypomyelination in the central nervous system (CNS) (7). Missense mutations in the proteolipid protein 1 (*PLP1*) gene cause a wide spectrum of clinical phenotypes from a mild allelic disease, spastic paraplegia type 2 (SPG2) to severe connatal PMD (7). In these diseases, mutant proteins are misfolded and accumulate in the ER, leading to induction of ER stress and apoptosis of oligodendrocytes in the CNS (8, 9). However, little is known about how different mutations in the same gene induce ER stress differently and affect clinical severity. Factors, such as retention of misfolded proteins or the extent of UPR activation, may influence phenotypic variation (9–11). However, can any other factors contribute to the pathology of such ER stress-related disease? Here we focused on ER chaperones as a potential player. ER chaperones are highly conserved proteins that assist in protein folding. Therefore, it is generally believed that accumulation of misfolded proteins in the ER up-regulates chaperones to alleviate ER stress. In terms of its association with disease pathology, interaction between the mutant PLP1 and a major ER chaperone, calnexin (CANX), was shown to inhibit degradation of the misfolded mutant proteins (12). In the mutant superoxide dismutase model of amyotrophic lateral sclerosis (ALS), an ER stress-associated neurodegenerative disease, down-regulation of another chaperone, calreticulin (CALR), was shown to induce ER stress and trigger the death of mutant superoxide dismutase motoneurons (13). A recent study reported up-regulation of protein-disulfide isomerase (PDI, also referred to as P4HB), which is a chaperone in the ER catalyzing the formation and breakage of protein disulfides bonds, in microglia of transgenic mutant superoxide dismutase 1 mice (14). Therefore, we sought to determine whether changes in the expression of ER chaperones alter the accumulation of misfolded protein and ER stress, potentially modifying the cellular and clinical phenotypes.

For this purpose, we used PMD as a model and investigated missense *PLP1* mutations (8, 11). PLP1 with an A243V substitution (PLP1msd) is representative of the severe hypomyelination in myelin synthesis deficit (*msd*) mice (15) and humans (16), whereas two other mutations, W163L and I187T, are representative of the milder condition found in mild PMD/SPG2 patients (17, 18): the latter is also the mutation found in an SPG2 mouse model, *rumpshaker* (19). We also employed mutants in two other genes responsible for peripheral myelin disorders, a myelin protein zero (MPZ) mutant associated with a severe neuropathy, Dejerine-Sottas neuropathy (20), and two peripheral myelin protein 22 (PMP22) mutants that are associated with a clinically mild neuropathy, Charcot-Marie-Tooth disease (21–23).

In this study, we examined the expression of ER chaperones in response to mutants of *PLP1* and two other genes. Unexpectedly, we found that some ER chaperones were depleted rather than up-regulated. In addition, these mutant proteins induced fragmentation of the Golgi apparatus (GA). We also found an association between these changes and phenotypic severity. Furthermore, we proposed potential mechanisms underlying these cellular phenotypes. The results of this study suggest that changes in these subcellular organelles may contribute to the cellular pathogenesis and phenotypic severity of inherited ER stress-related diseases caused by mutant proteins.

EXPERIMENTAL PROCEDURES

Mice—Msd mice, which carry the spontaneous A243V mutation in the *Plp1* gene (15), were maintained in a B6C3F1/J background in accordance with the institutional guidelines of the National Center of Neurology and Psychiatry.

Plasmid Construction—Expression vectors for PLP1wt and PLP1msd were reported previously (24). *PLP1-W163L* and *PLP1-I187T* genes were generated by site-directed mutagenesis with modifications (25), and subcloned into pCAGGS (24), as fusions with N-terminal FLAG epitopes. Human wild-type and mutant *PMP22* and *MPZ* genes were amplified from cloned cDNAs (kind gift from Dr. JR Lupski) using appropriate primers and inserted into pCAGGS. For construction of an expression vector for the membrane-linked cell surface green fluorescent protein (GFP) as illustrated in Fig. 9*E*. The *GFP* gene was inserted into pDisplay (Invitrogen) in an in-frame manner. The *cytoplasmic luciferase* (*Cluc*) and *immunoglobulin (Ig) κ light chain* (*Igκ-Rluc*) genes were amplified from cloned cDNA (Promega) with appropriate primers, and cloned into pCDNA3.1 (Invitrogen) and pAP-Tag5 (GenHunter) to construct pCMV-Cluc and pCMV-Igκ-Rluc, respectively. To determine subcellular localization, the *Rluc* gene was inserted in-frame between the Igκ and myc sequences of pAP-Tag5 to make pCMV-Igκ-Rluc-Myc. The mouse myelin oligodendrocyte glycoprotein (*MOG*) gene was also amplified with appropriate primers using cDNA from postnatal day (P) 14-mouse spinal cord (SC), and cloned into pEGFP-N1 (Takara).

Chemicals and Antibodies—The following reagents were purchased from the suppliers indicated: brefeldin A (Wako), tunicamycin (Merck), thapsigargin (Sigma), lactacystin (Wako), and MG132 (Wako). The primary antibodies included mouse anti-PDI (Thermo Scientific, MA3-019), rabbit anti-CALR (Sigma, C4606), rabbit anti-GRP78 (Abcome, ab21685), rabbit anti-CANX (Enzo Life Sciences, ADI-SPA-860), mouse anti-CHOP (Santa Cruz Biotechnology, sc-7351), rabbit anti-GM130 (Abcome, ab52649), mouse anti-FLAG M2 (Sigma, F3165), rabbit anti-FLAG M2 (Cell Signaling, number 2368), mouse anti-c-Myc (Nacalai Tesque, MC045), rabbit anti-PLP (a kind gift from Dr. M. Itoh, NCNP), rabbit anti-Oligo2 (IBL 18953), mouse anti-myelin basic protein (MBP) (Covance, SMI-99P), mouse anti-action (Millipore, MAB1501), rabbit

anti-KDEL receptor (Santa Cruz Biotechnology, sc-33806) and mouse anti-ubiquitin (Santa Cruz Biotechnology, sc-8017) antibodies. Alexa Fluor-488, -594, and -647 secondary antibodies were purchased from Invitrogen. Horseradish peroxidase-labeled anti-mouse and rabbit antibodies were purchased from GE Healthcare.

Cell Culture—HeLa cells and human oligodendrocytic cells (MO3.13) were maintained in Dulbecco's modified Eagle's medium (DMEM, Thermo Scientific) supplemented with 20 units ml^{-1} of penicillin, 20 $\mu g\ ml^{-1}$ of streptomycin, and 10% fetal bovine serum. For transfection, HeLa cells were plated onto 6-well plates or 18-mm round coverslips in 12-well plates, and transfected with the indicated constructs using Lipofectamine 2000 (Invitrogen) or TransIt LT1 (Mirus), respectively, according to the manufacturers' protocols. After 24 h, transfected cells in the 6-well plates or on coverslips were subjected to immunoblotting, quantitative PCR and immunocytochemistry, respectively.

Mixed Glial Culture (MGC) Generated to Oligodendrocyte—MGCs were established from wild-type and *msd* mice, which were then differentiated into oligodendrocytes, as described by Abematsu *et al.* (26).

Immunoblot Analysis—HeLa cells and mouse SCs were lysed with TNE(+) lysis buffer (50 mM Tris-HCl, pH 8.0, 150 mM NaCl, 2 mM EDTA, 1% Triton-X-100, and 0.1% SDS) supplemented with protease and phosphatase inhibitors on ice for 10 min. For the digitonin fractionation experiment, HeLa cells were permeabilized with phosphate-buffered saline (PBS) containing 0.01% digitonin with protease and phosphatase inhibitors on ice for 10 min. After soluble proteins were collected, insoluble proteins were further treated with the TNE(+) lysis buffer. These extracts were centrifuged at 12,000 × *g* for 10 min to remove cell debris. Co-immunoprecipitation and cell surface biotinylation were performed as described previously (27). The cell extracts, co-immunoprecipitation and biotinylated samples, were subjected to immunoblotting with primary antibodies and horseradish peroxidase-labeled secondary antibodies. All immunoblot analyses were repeated at least 3 times with similar results. The relative protein expression levels on immunoblotting were quantified by an image analyzer.

Immunocytochemistry—HeLa cells, MO3.13 cells, and primary oligodendrocytes were fixed with 4% paraformaldehyde in PBS for 10 min, permeabilized with 0.1% Triton X-100 for 10 min, and treated with 3% bovine serum albumin to block nonspecific reaction. Detection of cell surface proteins, cells were not permeabilized by 0.1% TritonX-100. Cells were further incubated with the primary antibodies for 60 min at RT followed by visualization using the appropriate secondary antibodies labeled with Alexa-488, -594, or -647 with 4′,6-diamidino-2-phenylindole (DAPI). Apoptotic cells were detected using ApopTag kit (Chemicon), according to the manufacturer's protocol. These stained cells were observed with a confocal fluorescence microscope (FV-1000; Olympus).

Quantitative Reverse Transcriptase-Polymerase Chain Reaction—Total RNA was extracted from HeLa cells and mouse SCs and was converted to cDNA using SuperScript III reverse transcriptase (Invitrogen). Transcript levels were analyzed by a thermal cycler (7900HT; Applied Biosystems) with synthesized cDNA and the following pre-designed TaqMan probes (Applied Biosystems): human *GAPDH*, Hs99999905; human *CHOP*, Hs00358796; human *P4HB*, Hs00168586; human *CALR*, Hs00189032; human *GRP78*, Hs99999174; human *CANX*, Hs00233492; mouse *Gapdh*, Mm99999915; mouse *Chop*, Mm00492097; mouse *P4hb*, Mm01243184; mouse *Calr*, Mm00482936; mouse *Grp78*, Mm00517691; and mouse *Canx*, Mm00500330. Relative transcript levels were calculated by the $\Delta\Delta C_T$ method according to the manufacturer's standard protocol.

Luciferase Reporter Assay—HeLa cells were co-transfected with the Cluc and Igκ-Rluc genes along with pCDNA3.1-PLP1wt-FLAG, pCDNA3.1-PLP1msd-FLAG, or the empty vector. Activities for firefly luciferase and Igκ-Rluc in the cell lysate and supernatant were measured using a dual-luciferase assay system (Promega) according to the manufacturer's instructions. Relative Cluc and Igκ-Rluc activities in the supernatant were determined as ratios to cytosolic luciferase activity.

Statistical Analysis—Student's *t* test and analysis of variance were used for statistical analyses.

RESULTS

PDI, CALR, and GRP78 Are Depleted in the ER of HeLa Cells Expressing PLP1msd—Typically, when cells are under ER stress, ER chaperones are up-regulated as a part of the UPR. ER chaperones improve cell survival by facilitating the correct folding or assembly of misfolded proteins and preventing their aggregation (28). In HeLa cells, FLAG-tagged PLP1msd (PLP1msd-FLAG), a PMD-causing severe mutant known to induce ER stress (8) but not FLAG-tagged wild-type PLP1 (PLP1wt-FLAG), effectively co-immunoprecipitated GRP78 (Fig. 1*A*) and up-regulated the *CHOP* gene (Fig. 1*B*), a well characterized ER stress marker gene, indicating that this transient transfection system is applicable for analyzing cellular pathogenesis of ER stress caused by exogenous mutant proteins. To further analyze the changes in ER chaperone expression induced by this mutant PLP1, transfected HeLa cells were immunostained with antibodies against the FLAG epitope, PDI, CALR, GRP78, and CANX. Unexpectedly, we found that PDI, CALR, and GRP78 were drastically depleted, whereas CANX expression was unchanged (Fig. 1*C*). These changes were also observed in the human oligodendrocytic cell line MO3.13 (Fig. 1*D*), the human glioma cell line U-138, and simian kidney cell line COS-7 cells (data not shown). Almost 65% of the cells transfected with PLP1msd-FLAG had faint PDI, CALR, and GRP78 staining. This proportion was significantly higher than in cells transfected with PLP1wt-FLAG (Fig. 1*E*), suggesting that this phenomenon is due to the mutant PLP1, not the overexpression of PLP1 itself.

Next, we determined if reduced chaperone expression is caused by apoptotic cell death due to overwhelming ER stress. Cells expressing PLP1msd that had faint PDI immunostaining had no positive signal in the terminal deoxynucleotidyl transferase dUTP nick-end labeling (TUNEL) assay (Fig. 1*F*). Furthermore, depletion of PDI occurred as early as 6 h after transfection (Fig. 1*G*). These results suggest that PLP1msd impairs the ER chaperones independent of apoptosis.

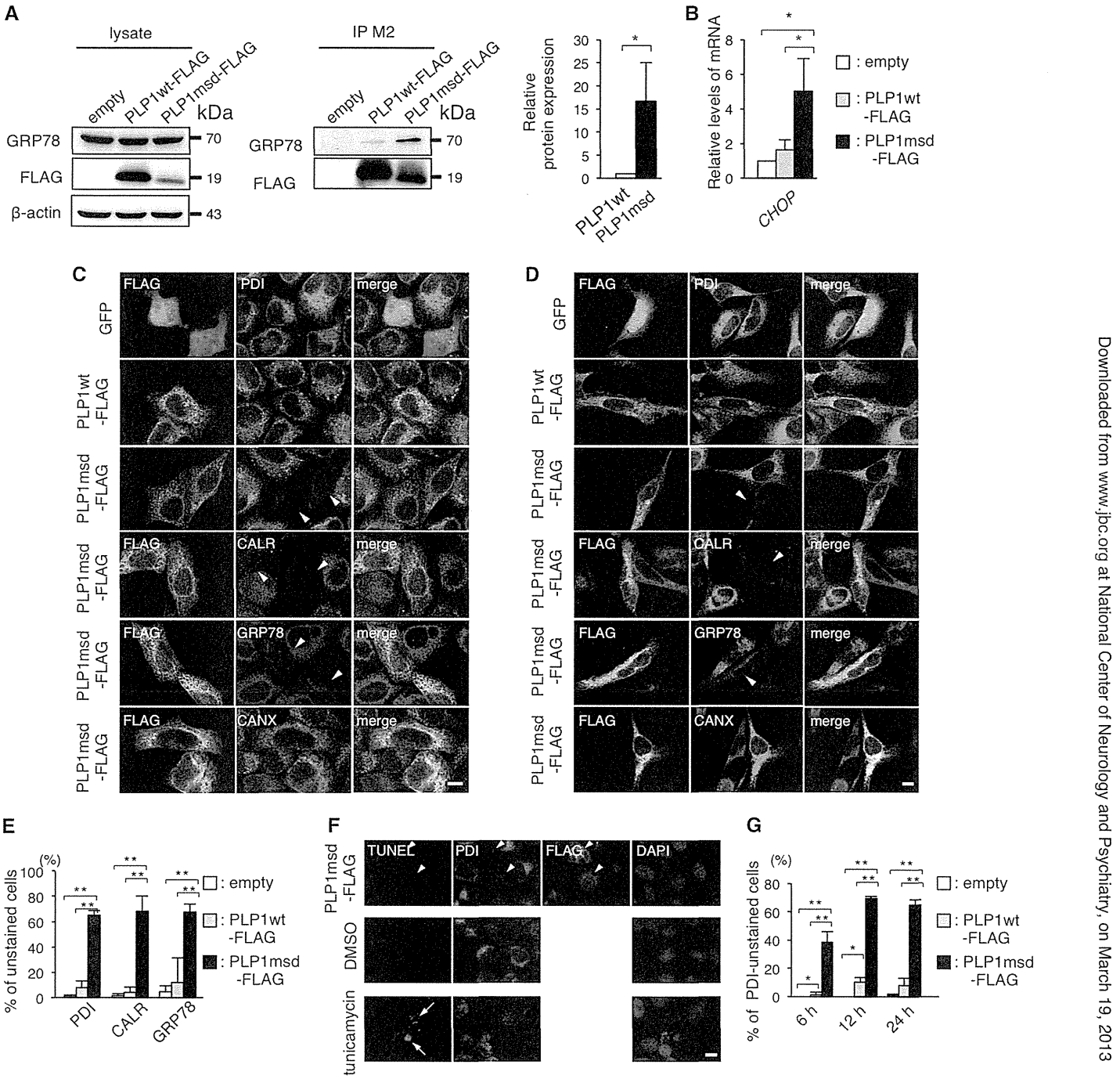

FIGURE 1. **PLP1msd overexpression resulted in a negative ER chaperone staining pattern.** *A*, co-immunoprecipitation of PLP1 with GRP78 in HeLa cells. *B*, quantitative RT-PCR for the *CHOP* gene in HeLa cells expressing PLP1wt or PLP1msd. The *GAPDH* gene was used as an internal control. Results are represented as fold-induction compared with empty vector-transfected control experiment. Values are represented as the mean ± S.E. from three independent experiments (*, $p \leq 0.05$). *C* and *D*, immunocytochemistry of ER chaperones in HeLa cells (*C*) and human oligodendrocytic cells, and MO3.13 cells (*D*) expressing PLP1wt or PLP1msd. Cells transfected with the indicated vectors were immunostained with an anti-FLAG antibody (*green*) together with anti-PDI, anti-CALR, anti-GRP78, or anti-CANX antibodies (*magenta*) and observed with a confocal fluorescence microscope. Note that cells expressing PLP1msd showed an extremely faint staining pattern (*arrowheads*) for PDI, CALR, and GRP78, but not for CANX. *Scale bar*, 10 μm. *E*, the proportion of unstained cells for PDI, CALR, and GRP78. *F*, apoptosis of HeLa cells expressing PLP1msd. TUNEL assay combined with immunocytochemical staining using the anti-FLAG (*white*) and anti-PDI (*magenta*) antibodies. Tunicamycin treatment served as a positive control for TUNEL (*arrow*). None of the PLP1msd-positive cells showed positive signals for TUNEL (*arrowheads*). *Scale bar*, 10 μm. *G*, time course of the proportion of PDI negative HeLa cells transfected with the PLP1msd gene. The results are represented as the mean ± S.E. from three independent experiments with >100 cells counted in each experiment (*, $p \leq 0.05$; **, $p \leq 0.005$).

Expression of PLP1msd Translocates the ER Chaperones from the ER—To examine whether PLP1msd depletes the chaperones by inhibiting their transcription in HeLa cells, we performed quantitative real time-polymerase chain reaction (RT-PCR) (Fig. 2*A*). As we demonstrated previously (24), *GRP78* mRNA expression was increased significantly in cells transfected with PLP1msd-FLAG compared with cells transfected with PLP1wt-FLAG. The expression of *PDI* and *CALR* was slight, but significantly up-regulated. These results indicate that PDI, CALR, and GRP78 are depleted in the ER without

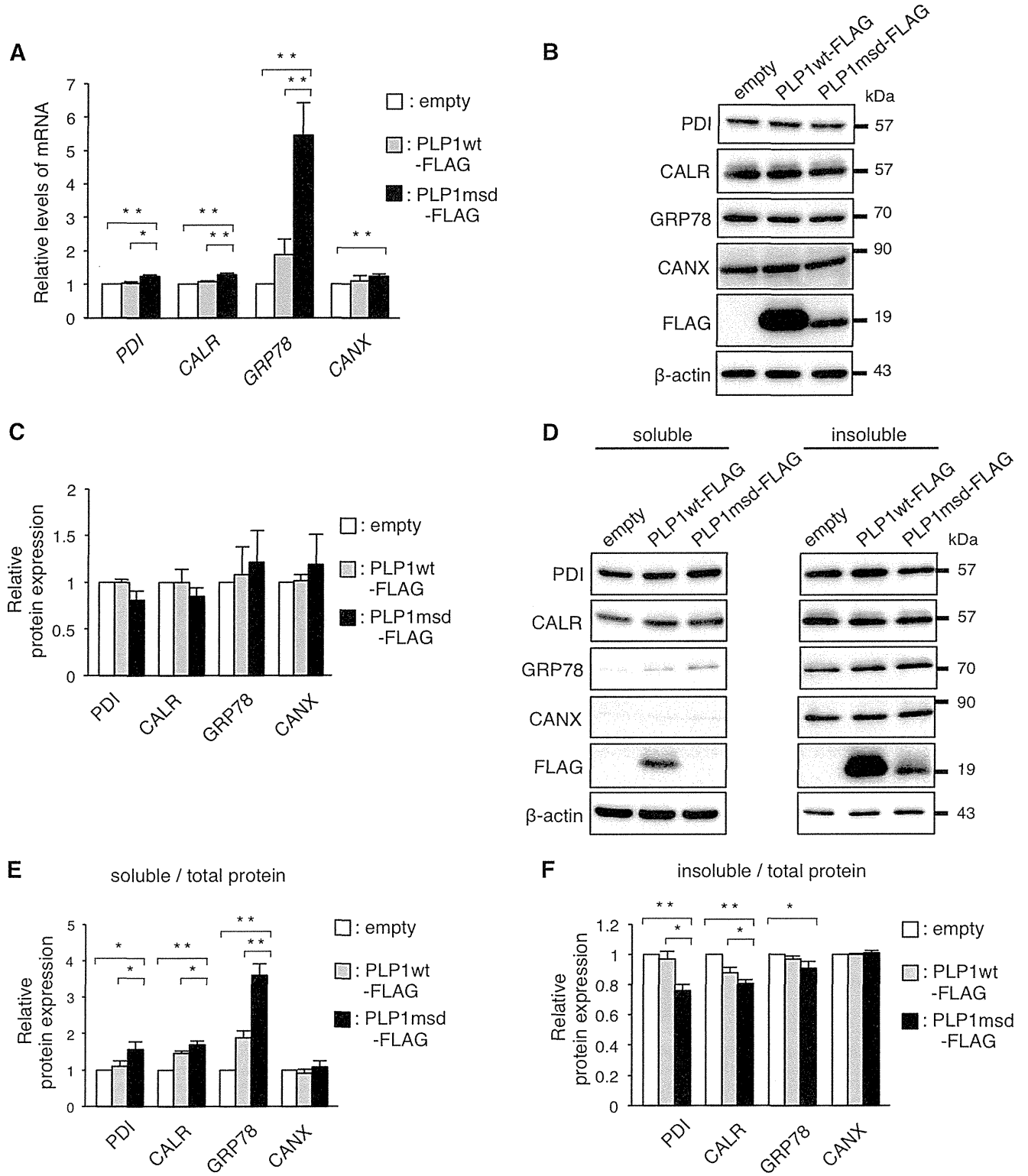

FIGURE 2. **PDI, CALR, and GRP78 are depleted from the ER without decreasing their transcripts.** *A*, relative expression of the transcripts of the ER chaperones in HeLa cells transfected with the PLP1 genes. Expression levels of *PDI*, *CALR*, *GRP78*, and *CANX* mRNA were analyzed by quantitative RT-PCR and normalized to *GAPDH*. The results are represented as fold-induction against the control experiment (empty vector transfection). *B* and *C*, total amount of the ER chaperones in HeLa cells transfected with PLP1wt-FLAG and PLP1msd-FLAG. Protein samples from the cells transfected with the indicated vectors were subjected to immunoblotting with the indicated antibodies (*B*). The amounts of the proteins were measured by densitometry and normalized to β-actin. The results are represented as fold-induction against the control experiment using the empty vector (*C*). *D–F*, subcellular fractionation analysis using 0.01% digitonin. Transfected cells were treated with 0.01% digitonin followed by 0.1% SDS, 1% Triton X-100. The extracts of digitonin soluble (*left*) and insoluble fraction (*right*) were subjected to immunoblotting with the indicated antibodies (*D*). The blots were quantitatively analyzed by densitometry to measure the proportion of soluble fraction (*E*) and insoluble fraction (*F*) in each protein. Bar graphs are represented as fold-induction ± S.E. against the mean of control experiment from three independent experiments (*, $p \leq 0.05$; **, $p \leq 0.005$).

decreasing their transcription. Furthermore, total protein levels of these chaperones were essentially unchanged in cells transfected with PLP1msd-FLAG (Fig. 2, *B* and *C*). These results indicate that PDI, CALR, and GRP78 depletion in the ER is not due to a reduction in the total proteins.

Next, we considered the possibility that PLP1msd affected subcellular localization of the ER chaperones from the ER to another cellular compartment. To test this possibility, transfected cells were treated with 0.01% digitonin, which permeabilizes the plasma membrane but not organelles' membranes, followed by treatment with 0.1% SDS, 1% Triton X-100, which permeabilizes the organelles, including the ER (Fig. 2, *D–F*). In cells expressing PLP1msd, the proportion of PDI, CALR, and GRP78 in the fraction containing the plasma membrane and cytosol (soluble fraction) was higher than in cells expressing PLP1wt (Fig. 2, *D* and *E*). In contrast, the amount of these chaperones was lower in fractions containing the ER (insoluble fraction) in PLP1msd expressing cells (Fig. 2, *D* and *F*). Interestingly, the amount of CANX was unchanged in the digitonin-soluble and -insoluble fractions. These results suggest that the decrease in PDI, CALR, and GRP78 in the ER may be due to their translocation from the ER to the plasma membrane or cytosol, but not due to the decrease of total protein.

Recently, Zhang *et al.* (29) reported that ER stress actively promotes GRP78 localization on the cell surface. We confirmed that thapsigargin, a well known ER stressor, increases cell surface expression of PDI in HeLa cells by immunocytochemistry (Fig. 3*A*) and increases cell surface expression of GRP78 and PDI in HeLa cells by cell surface biotinylation (Fig. 3*C*). However, we observed no expression of PDI on the cell surface of PLP1msd-transfected cells (Fig. 3*B*) or no increment of the biotinylated PDI, CALR, and GRP78 in these cells (Fig. 3*D*). These findings suggest that these mutant proteins induce translocation of the chaperones from the ER to the cytosol, rather to the cell surface.

We speculated that mislocalized cytoplasmic chaperons are degraded through a ubiquitin-dependent ERAD pathway. However, although the amounts of ubiquitinated proteins increased in the presence of proteasome inhibitors, MG-132 or lactacystin (Fig. 3*F*), those of the ER chaperons were not affected (Fig. 3*E*), suggesting that they are not degraded through the ERAD pathway after releasing to the cytosol.

Differences and Similarities among Disease-causing Mutations in Other Myelin Genes—To determine whether the depletion of chaperone proteins from the ER is unique to the mutant PLP1 protein or is a common phenomenon observed with mutant proteins encoded by other disease-causing genes, we also examined *PMP22* and *MPZ* genes. Mutations in these genes cause a spectrum of autosomal dominant peripheral demyelinating neuropathies (30).

First, to determine whether accumulation of misfolded proteins in the ER is sufficient to reduce ER chaperone proteins to undetectable levels (by immunostaining) in HeLa cells, we examined two representative PMP22 mutants, *Trembler-J* (*Tr-J*) (an L16P substitution) and *Trembler* (*Tr*) (a G150D substitution), both of which accumulate in the ER by associating with CANX, however, do not induce UPR (31). Both of *Tr-J* and *Tr* are found in humans (32, 33) and mice (34, 35). First, we found no increase in the immunoreactivity of CHOP, which is one of the universal markers of ER stress (36), in either Tr or Tr-j, confirming that these mutants evoked no ER stress (Fig. 4*B*). We then performed immunocytochemistry with the anti-PDI (Fig. 4, *A* and *C*), anti-CALR, and anti-GRP78 (CALR, GRP78, data not shown) antibodies in HeLa cells transfected with the PMP22wt or mutant PMP22 genes. In contrast to our findings in cells transfected with the mutant PLP1 gene, we observed no depletion of these chaperones from the ER in cells expressing the mutant PMP22. These findings indicate that ER accumulation of these mutant proteins, which trigger no ER stress, is insufficient to induce depletion of ER chaperones from the ER.

Next, to analyze whether mutations in another gene that triggers ER stress also deplete the chaperones from the ER, we performed the same experiments using an *MPZ* gene harboring the 506delT mutation (MPZ506delT), which induces ER stress and causes a more severe form of peripheral neuropathy, Dejerine-Sottas neuropathy. This frameshift mutation results in 82 residues of shifted amino acid sequence starting from codon 169 in the MPZ protein (20). CHOP immunofluorescence was increased in the nucleus of HeLa cells transfected with the MPZ506delT gene, but not in cells transfected with the wild-type MPZ gene (MPZwt) (Fig. 4*E*), confirming that this mutant protein is an ER stressor. Immunocytochemistry (Fig. 4*D*) showed that the MPZ506delT mutant, but not MPZwt, increased the number of cells unstained with anti-PDI antibody (Fig. 4*F*). These results strongly suggested that depletion of the chaperones from the ER is not induced solely by protein accumulation in the ER, but instead requires both the accumulation of particular mutant proteins and ER stress. In addition, mutations in disease-causing genes other than *PLP1* can elicit the chaperone depletion.

Depletion of PDI, CALR, and GRP78 Is Linked to PMD Severity—Because ER chaperones are connected with protein folding in the ER, we hypothesized that depletion of the ER chaperones may affect the pathogenesis or severity of PMD. We employed two PLP1 mutants, W163I (11) and I187T (18), both of which result in the mild end of the clinical spectrum of PMD (Fig. 5*A*). Densitometric analysis of CHOP immunofluorescence in transfected HeLa cells confirmed that these milder PLP1 mutants activated the UPR, but to a lesser extent than cells transfected with the PLP1msd gene (Fig. 5*B*).

Next, to analyze whether ER chaperone depletion is associated with clinical severity, we compared the expression of PDI in HeLa cells transfected with these PLP1 mutant genes. We found that the proportion of PDI-unstained cells expressing FLAG-tagged PLP1-W163L or PLP1-I187T was significantly lower than that of cells expressing PLP1msd (Fig. 5*C*). In addition, we observed a similar tendency in cells expressing the MPZ mutants. A mild MPZ allele, MPZS63del, evoked less ER stress and resulted in a smaller proportion of "PDI-unstained cells" than a severe allele, MPZ506delT (data not shown). Together, these results strongly suggest a potential linkage between chaperone depletion and the phenotypic variation in ER stress-related disorders.